

Medium Effects in Neutrino Cooling of Neutron Stars^{*}

Dmitri N. Voskresensky

Moscow Institute for Physics and Engineering, Russia, 115409 Moscow,
Kashirskoe shosse 31; Gesellschaft für Schwerionenforschung GSI, P.O.Box
110552, D-64220 Darmstadt, Germany

Abstract. This review demonstrates that neutrino emission from dense hadronic component in neutron stars is subject of strong modifications due to collective effects in the nuclear matter. With the most important in-medium processes incorporated in the cooling code an overall agreement with available soft X ray data can be easily achieved. With these findings so called "*standard*" and "*non-standard*" cooling scenarios are replaced by one general "*nuclear medium cooling scenario*" which relates slow and rapid neutron star coolings to the star masses (interior densities). In-medium effects take important part also at early hot stage of neutron star evolution decreasing the neutrino opacity for less massive and increasing for more massive neutron stars. A formalism for calculation of neutrino radiation from nuclear matter is presented that treats on equal footing one-nucleon and multiple-nucleon processes as well as reactions with resonance bosons and condensates.

1 Introduction

The EINSTEIN, EXOSAT and ROSAT observatories have measured surface temperatures of certain neutron stars (NS) and put upper limits on the surface temperatures of some other NS (cf. [1–3] and further references therein). The data for some supernova remnants indicate rather slow cooling, while the data for several pulsars point to an essentially more rapid cooling.

Physics of NS cooling is based on a number of ingredients, among which the neutrino emissivity of the high density hadronic matter in the star core plays a crucial role. Neutron star temperatures are such that, except first minutes–hours, neutrinos/antineutrinos radiate energy directly from the star without subsequent collisions, since $\lambda_\nu, \lambda_{\bar{\nu}} \gg R$, where $\lambda_\nu, \lambda_{\bar{\nu}}$ are the neutrino and antineutrino mean free paths and R is star radius. In the so called "*standard scenario*" of the NS cooling (scenario for slow cooling) the most important channel up to temperatures $T \sim 10^9$ K belongs to the modified Urca (MU) process $nn \rightarrow npe\bar{\nu}$. First estimates of its emissivity were done in [4,5]. References [6,7] recalculated the emissivity of this process in the model, where the nucleon-nucleon (NN) interaction was treated with the help of slightly modified free one-pion exchange (FOPE). This important result for

^{*} Invited talk at Intern. Workshop on Phys. of Neutron Star Interiors, Trento, June 2000

the emissivity, $\varepsilon_\nu[\text{FOPE}]$, was proved to be by an order of magnitude larger than the previously obtained one. Namely the value $\varepsilon_\nu[\text{FOPE}]$ was used in various computer simulations resulting in the "*standard scenario*" of the cooling, e.g. cf. [8–10]. Besides the MU process, in the framework of the "*standard scenario*" numerical codes included also processes of the nucleon (neutron and proton) bremsstrahlung (NB) $nn \rightarrow nn\nu\bar{\nu}$ and $np \rightarrow np\nu\bar{\nu}$, which lead to a smaller contribution to the emissivity than the MU, cf. [11,6]. Medium effects enter the above two-nucleon (MU and NB) rates mainly through the effective mass of the nucleons which has a smooth density dependence. Therefore within FOPE model the density dependence of the reaction rates is rather weak and the neutrino radiation from a NS depends only very weakly on its mass. This is the reason why the "*standard scenario*" based on the result [6], though complying well with several slowly cooling pulsars, fails to explain the data of the more rapidly cooling ones. Also "*standard scenario*" included processes contributing to the emissivity in the NS crust which become important at a lower temperature.

The *non-standard scenario* included so called exotica, associated with different types of direct Urca-like processes, i.e. the pion Urca (PU) [12] and kaon Urca (KU) [13,14] β -decay processes and direct Urca (DU) on nucleons and hyperons [15] possible only in sufficiently dense interiors of rather massive NS. The main difference in the cooling efficiency driven by the DU-like processes on one hand and the MU and NB processes on the other hand lies in the rather different phase spaces associated with these reactions. In the MU and NB case the available phase space is that of a two-fermion origin, while in the pion (kaon) β -decay and DU on nucleons and hyperons it is that of a one-fermion origin. Critical density of pion condensation in NS matter is $\varrho_{c\pi} \simeq (1 \div 3)\varrho_0$ depending on the type of condensation (neutral or charged) and the model, see [16–19]. Critical density of kaon condensation is $\varrho_{cK} \simeq (2 \div 6)\varrho_0$ depending on the type (K^- or \bar{K}^0 , S or P wave) and the model, see [20,21]. Critical density for the DU process is $\varrho_{cU} \simeq (2 \div 6)\varrho_0$ depending on the model for the equation of state (EQS), see [15,18]. Recent calculations [19] estimated critical density of neutral pion condensation as $2.5\varrho_0$ and for the charged one as $1.7\varrho_0$, whereas variational calculations [18] argued even for smaller critical densities ($\simeq 1.3\varrho_0$ for π^0 condensation). On the other hand the EQS of [18] allows for DU process only at $\varrho > 5\varrho_0$.

There is no bridge between "*standard*" and "*non-standard*" scenarios due to complete ignorance of in-medium modifications of NN interaction which allows for strong polarization of the soft modes (like virtual dressed pion and kaon modes serving a part of in-medium baryon–baryon interaction). Only due to enhancement of such a polarization with the baryon density mentioned condensates may appear and it seems thereby quite inconsistent to ignore these softening effects for $\varrho < \varrho_{c\pi}, \varrho_{cK}$, and suddenly switch on the condensates for $\varrho > \varrho_{c\pi}, \varrho_{cK}$.

Now let us basing on the results [22–25,16,26] briefly discuss a general “*nuclear medium cooling scenario*” which treats obvious caveats of two mentioned above scenarios. First of all one observes [22] that in the nuclear matter many new reaction channels are opened up compared to the vacuum processes. Standard Feynman technique fails to calculate in-medium reaction rates if the particle widths are important since there are no free particle asymptotic states in matter. Then summation of all perturbative Feynman diagrams where free Green functions are replaced by the in-medium ones leads to a double counting due to multiple repetitions of some processes (for an extensive discussion of this defect see [27]). This calls a formalism dealing with closed diagrams (integrated over all possible in-medium particle states) with full non-equilibrium Green functions. Such a formalism was elaborated in [23,24] first within quasiparticle approximation (QPA) for nucleons and was called in [24] “*optic theorem formalism (OTF) in non-equilibrium diagram technique*”. It was demonstrated that standard calculation of the rates via squared reaction matrix elements and calculation using OTF coincide within QPA picture for the fermions. In [28] the formalism was generalized to include arbitrary particle widths effects. The latter formalism treats on equal footing one-nucleon and multiple-nucleon processes as well as resonance reaction contributions of the boson origin, as processes with participation of zero sounds and reactions on the boson condensates. Each diagram in the series with full Green functions is free from the infrared divergences. Both, the correct quasiparticle (QP) and quasiclassical limits are recovered.

Except for very early stage of NS evolution (minutes - hours) typical averaged lepton energy ($\gtrsim T$) is larger then the nucleon particle width $\Gamma_N \sim T^2/\varepsilon_{FN}$ and the nucleons can be treated within the QPA. This observation much simplifies consideration since one can use an intuitive way of separation of the processes according to the available phase space. The one-nucleon processes have the largest emissivity (if they are not forbidden by energy-momentum conservations), then two-nucleon processes come into play, etc.

In the temperature interval $T_c < T < T_{opac}$ (T_c is typical temperature for the nucleon pairing and T_{opac} is typical temperature at which neutrino/antineutrino mean free path $\lambda_\nu/\lambda_{\bar{\nu}}$ is approximately equal to the star radius R) the neutrino emission is dominated by the medium modified Urca (MMU) and medium nucleon bremsstrahlung (MNB) processes if one-nucleon reactions like DU, PU and KU are forbidden, as it is the case for $\varrho < \varrho_{cU}, \varrho_{c\pi}, \varrho_{cK}$. Corresponding diagrams for MMU process are schematically shown in Fig. 1. References [22–25,16] considered NN interaction within Fermi liquid Landau–Migdal approach. They incorporated the softening of the medium one-pion exchange (MOPE) mode, other medium polarization effects, like nucleon-nucleon correlations in the vertices, renormalization of the local part of NN interaction by the loops, as well as the possibility of the neutrino emission from the intermediate reaction states and resonance DU-like reactions going on zero sounds and the boson condensates. Refer-

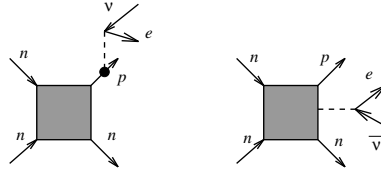


Fig. 1. Antineutrino emission from a nucleon leg (left graph) and from intermediate scattering states (right) in MMU process. Full dot includes weak coupling vertex renormalization.

ences [23,25,16] have demonstrated that for $\varrho \gtrsim \varrho_0$ second diagram of Fig. 1 gives the main contribution to the emissivity of MMU process rather than the first one which contribution has been earlier evaluated in the framework of FOPE model in [6]. This fact essentially modifies the absolute value as well as the density dependence of the $nn \rightarrow npe\bar{\nu}$ process rate which becomes to be very sharp. Thereby, for stars of masses larger than the solar mass the resulting emissivities were proved to be substantially larger than those values calculated in FOPE model. With increase of the star mass (central density) pion mode continues to soften and MMU and MNB rates still increase. At $\varrho > \varrho_{c\pi}$ pion condensation begins to contribute. Actually, the condensate droplets exist already at a smaller density in the mixed phase appearing in systems having more than one conserved charge [29,30]. At $T > T_{melt}$, where T_{melt} is the melting temperature, roughly \sim several MeV, the mixed phase is in liquid state and PU processes on independent condensate droplets are possible. At $T < T_{melt}$ condensate droplets are placed in a crystalline lattice that substantially suppresses corresponding neutrino processes.

Reference [12] considered the reaction channel $n \rightarrow p\pi_c^- e\bar{\nu}$, whereas [22,23] included other possible pion π^+ , π^\pm , π^0 condensate processes with charged and neutral currents (e.g., like $n\pi_c^0 \rightarrow pe\bar{\nu}$, $n\pi_c^+ \rightarrow p\nu\bar{\nu}$ and $n\pi_c^0 \rightarrow n\nu\bar{\nu}$) as well as resonance reactions going on zero sounds which are also possible at $\varrho < \varrho_{c\pi}$. Due to NN correlations all pion condensate rates are significantly suppressed (by factors $\sim 10 - 100$ compared to first estimate [12], see [31,22,23,32]. At $\varrho \sim \varrho_{c\pi}$ both MMU and PU processes are of the same order of magnitude [23] demonstrating a smooth transition to higher densities (star masses) being absent in the "standard" and "non-standard" scenarios.

For $T < T_c$ the reactions of neutrino pair radiation from superfluid nucleon pair breaking and formation (NPBF) shown in Fig. 2 become to be dominant processes. The neutron pair breaking and formation (nPBF) process for the case of the $1S_0$ pairing was first calculated in [33] using standard Bogolyubov technique. Later this process was independently calculated in [24,25] as demonstration of efficiency of OTF within the closed non-equilibrium diagram technique developed there. Moreover [24] calculated emissivity of the corresponding process on proton (pPFB) taking into account strong coupling $p\nu\bar{\nu}$ vertex renormalization (see first diagram (17) below).

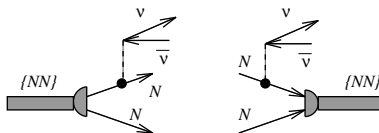


Fig. 2. Neutrino–antineutrino emission from Cooper pair-breaking (left graph) and pair-formation processes (right graph).

It results in one-two order of magnitude enhancement of pPFB emissivity compared to that would be estimated with the vacuum vertex, leading to that both nPFB and pPFB emissivities can be of the same order of magnitude. Emissivities of NPBF processes have the same suppression factor $\sim \exp(-2\Delta/T)$ as MU, NB, MMU and MNB at $T < T_c$ but compared to the latter the NPBF processes have a large one nucleon phase space volume. References [34,35] included peculiarities of $3P_2$ pairing. In the $3P_2(|m_J|=2)$ case, where m_J is projection of the total pair momentum onto quantization axis, exponential suppression of the specific heat and the emissivity is replaced by only a power law suppression since the gap vanishes at the Fermi sphere poles, the possibility first remarked in [24] and then in [16].

At this instance I would like to do a historic remark relating to estimation of the NPBF processes since in some works (e.g., see [36,35]) was expressed a surprise why these processes were not on a market during many years. First work [33], although found correct analytic expression for $1S_0$ pairing of neutrons, numerically underestimated the emissivity by an order of magnitude. Also there was no statement on the dominance of the process in the cooling scenario (i.e. over the MU). Asymptotic behaviour of the emissivity $\varepsilon[\text{nPBF}] \sim 10^{20} T_9^7 \exp(-2\Delta/T)$ for $T \ll \Delta$, $T_9 = T/10^9 \text{K}$, as follows from expression (1b) of [33] and from their rough asymptotic estimate of the integral (see below (13b)), shows up nor a large one nucleon phase space factor ($\sim 10^{28}$) nor appropriate temperature behaviour. Namely this underestimation of the rate in [33] (we again point out that analytic expression (1a) is correct) and absence of mentioning of possible dominance of the process over MU, became the reason that this important result was overlooked during many years. Reference [24] overlooked sign of anomalous diagram for S pairing and included $\propto g_A^2$ term (g_A is axial-vector coupling constant) which should be absent for S pairing giving, nevertheless, the main contribution for the $3P_2$ pairing case. A reasonable numerical estimate of the emissivity was presented valid for both S and P pairings including NN correlation effects into consideration. Uncertainty of this estimate is given by a factor $(0.5 \div 2)$ which is allowed by variation of not too well known correlation factors. Namely this estimate was then incorporated within the cooling code in [26]. Correct asymptotic behaviour of the emissivity is $\varepsilon[\text{nPFB}, \text{pPFB}] \sim 10^{28} (\Delta/\text{MeV})^7 (T/\Delta)^{1/2} \exp(-2\Delta/T)$ for $T \ll \Delta$, that showed up a huge one-nucleon phase space factor and very moderate T dependence of the pre-factor. Thereby the value of the rate was related

in [24] to the value of the pairing gap. The possibility of the dominant role of this process (even compared to enhanced MMU and PU rather than only MU) was unambiguously stressed. Unfortunately [24] had a number of obvious misprints which were partially corrected in subsequent papers. Although it does not excuse the authors these misprints can be easily treated by an *attentive* reader. Importance of NPFB processes was then once more stressed in review [16]. Reference [26] was the first that quoted the previous result [33]. It incorporated most important in-medium effects in the cooling code, among them nPBF and pPBF as equally important processes. However importance of pPBF process was then overlooked in the subsequent papers where emissivity of this process was several times incorrectly reproduced. Work [36] supported conclusion of [26] on importance of NPFB processes as governing the cooling scenario at $T < T_c$.

The medium modifications of all the above mentioned rates result in a pronounced density dependence (for NPBF processes mainly via dependence of the pairing gaps on the density and dependence on the NN correlation factors), which links the cooling behavior of a neutron star decisively to its mass [22,23,16,26]. As the result, the above mentioned medium modifications lead to a more rapid cooling than obtained in the "*standard scenario*". Hence they provide a possible explanation for the observed deviations of some of the pulsar temperatures from the "*standard*" cooling. Particularly, they provide a smooth transition from "*standard*" to "*non-standard*" cooling for increasing central star densities, i.e., star masses. Thus by means of taking into account of most important in-medium effects in the reaction rates one is indeed able to achieve an appropriate agreement with both the high as well as the low observed pulsar temperatures that leads to the new "*nuclear medium cooling scenario*". Using a collection of modern EQS for nuclear matter, which covered both relativistic as well as non-relativistic models, [26] also has demonstrated a relative robustness of these in-medium cooling mechanisms against variations in the EQS of dense NS matter.

At initial stage ($T > T_{opac}$) the newly formed hot NS is opaque for neutrinos/antineutrinos. Within FOPE model the value T_{opac} was estimated in [6]. Elastic scatterings were included in [37,38] and pion condensation effect on the opacity was discussed in [39]. Medium effects dramatically affect the neutrino/antineutrino mean free paths, since $\lambda_{\nu(\bar{\nu})} \propto 1/|M|^2$, where M is the reaction matrix element. Thereby, one-nucleon elastic scattering processes, like $N\nu \rightarrow N\nu$, for energy and momentum transfer $\omega < qv_{FN}$ are suppressed by NN correlations [24,16,40,41]. Neutrino/antineutrino absorption in two-nucleon MMU and MNB processes is substantially increased with the density (since $|M|^2$ for MMU and MNB processes increases with the density) [23,24,16]. Thus more massive NS are opaque for neutrinos up to lower temperatures that also results in a delay of neutrino pulse. Within the QPA for the nucleons the value T_{opac} was estimated with taking into account of medium effects in [23,16]. References [42,43,16] considered possible

consequences of such a delay for supernova explosions. On the other hand, at $T > (1 \div 2)\text{MeV}$ one should take care of the neutrino/antineutrino radiation in multiple NN scatterings (Landau–Pomeranchuk–Migdal (LPM) effect) when averaged neutrino–antineutrino energy, $\omega_{\nu\bar{\nu}} \sim \text{several } T$, becomes to be smaller than the nucleon width Γ_N [28]. Numerical evaluations of Γ_N in application to MNB processes were done in [44] and [45] within the Brückner scheme and the Bethe–Salpeter equation, respectively. The LPM effect suppresses the rates of the neutrino elastic scattering processes on nucleons and also it suppresses MNB rates. For NS of rather low mass ($\lesssim M_\odot$) the suppression of the rates of neutral current processes due to the multiple collision coherence effect prevails over the enhancement due to the pion softening, and for sufficiently massive NS ($\gtrsim 1.4M_\odot$) the enhancement prevails the suppression. MMU emissivity remains to be almost unaffected by the LPM effect since averaged $\bar{\nu}e$ energy $\sim p_{Fe}$ is rather large ($\gg \Gamma_N$).

The paper is organized as follows. Sect. 2 discusses basic ideas of the Fermi liquid approach to description of nuclear matter. The NN interaction amplitude is constructed with an explicit treatment of long-ranged soft pion mode and vertex renormalizations due to NN correlations. The meaning of the pion softening effect is clarified and a comparison of MOPE and FOPE models is given. Also renormalization of the weak interaction in NS matter is performed. Sect. 3 discusses the cooling of NS at $T < T_{\text{opac}}$. Comparison of emissivities of MMU and MU processes shows a significant enhancement of in-medium rates. Then we discuss DU-like processes and demonstrate medium effect due to vertex renormalizations. The role of in-medium mechanisms in the cooling evolution of NS is then demonstrated within a realistic cooling code. Next we consider influence of in-medium effects on the neutrino mean free path at initial stage of NS cooling. Essential role of multiple NN collisions is discussed. Sect. 4 presents OTF in non-equilibrium closed diagram technique in the framework of QPA for the nucleons and also beyond the QPA incorporating genuine particle width effects.

2 Nuclear Fermi liquid description

2.1 NN interaction. Separation of hard and soft modes

At temperatures of our interest ($T \ll \varepsilon_{Fn}$) neutrons are only slightly excited above their Fermi sea and all the processes occur in a narrow vicinity of ε_{Fn} . In such a situation Fermi liquid approach seems to be the most efficient one. Within this approach the long-ranged diagrams are treated explicitly whereas short-scale diagrams are supposed to be the local quantities given by phenomenological so called Landau-Migdal (LM) parameters. Thus using argumentation of Fermi liquid theory [46–48,16] the retarded NN interaction

amplitude is presented as follows (see also [49])

$$\text{Diagram} = \text{Diagram}_1 + \text{Diagram}_2 + \text{Diagram}_3 \quad (1)$$

where

$$\text{Diagram} = \text{Diagram}_1 + \text{Diagram}_2 \quad (2)$$

The solid line presents the nucleon, whereas double-line, the Δ isobar. The double-wavy line corresponds to the exchange of the free pion with inclusion of the contributions of the residual S wave πNN interaction and $\pi\pi$ scattering, i.e. the residual irreducible interaction to the nucleon particle-holes and delta-nucleon holes. The full particle-hole, delta-nucleon hole and pion irreducible block (first block in (2)) is by its construction essentially more local then contributions given by explicitly presented graphs. Thereby, it is parameterized with the help of the LM parameters. In the standard Landau Fermi liquid theory fermions are supposed to be at their Fermi surface and the Landau parameters are further expanded in Legendre polynomials in the angle between fermionic momenta. Luckily, only zero and first harmonics enter physical quantities. The momentum dependence of the residual part of nuclear forces is expected to be not as pronounced and one can avoid this expansion. Then these parameters, i.e. f_{nn} , f_{np} and g_{nn} , g_{np} in scalar and spin channels respectively, are considered as slightly momentum dependent quantities. In principle, they should be calculated as functions of the density, neutron and proton concentrations, energy and momentum but, simplifying, one can extract them from analysis of experimental data.

The part of interaction involving Δ isobar is analogously constructed

$$\text{Diagram} = \text{Diagram}_1 + \text{Diagram}_2 \quad (3)$$

The main part of the $N\Delta$ interaction is due to the pion exchange. Although information on local part of the $N\Delta$ interaction is rather scarce one can conclude [16,19] that the corresponding LM parameters are essentially smaller then those for NN interaction. Besides, at small transferred energies $\omega \ll m_\pi$ the Δ -nucleon hole contribution is a smooth function of ω and k in difference with the nucleon-nucleon hole (NN^{-1}) contribution. Therefore and also for simplicity we neglect the first graph in r.h.s. of (3).

Straightforward resummation of (1) in neutral channel yields [24,16]

$$\Gamma_{\alpha\beta}^R = \text{Diagram} = C_0 (\mathcal{F}_{\alpha\beta}^R + \mathcal{Z}_{\alpha\beta}^R \boldsymbol{\sigma}_1 \cdot \boldsymbol{\sigma}_2) + f_{\pi N}^2 \mathcal{T}_{\alpha\beta}^R (\boldsymbol{\sigma}_1 \cdot \mathbf{k})(\boldsymbol{\sigma}_2 \cdot \mathbf{k}), \quad (4)$$

$$\begin{aligned}
\mathcal{F}_{\alpha\beta}^R &= f_{\alpha\beta}\gamma(f_{\alpha\beta}), \quad \mathcal{Z}_{nn}^R = g_{nn}\gamma(g_{nn}), \quad \mathcal{Z}_{np}^R = g_{np}\gamma(g_{nn}), \quad \alpha, \beta = (n, p), \\
\mathcal{T}_{nn}^R &= \gamma^2(g_{nn})D_{\pi^0}^R, \quad \mathcal{T}_{np}^R = -\gamma_{pp}\gamma(g_{nn})D_{\pi^0}^R, \quad \mathcal{T}_{pp}^R = \gamma_{pp}^2 D_{\pi^0}^R, \\
\gamma^{-1}(x) &= 1 - 2xC_0A_{nn}^R, \quad \gamma_{pp} = (1 - 4gC_0A_{nn}^R)\gamma(g_{nn}),
\end{aligned} \tag{5}$$

$f_{nn} = f_{pp} = f + f'$, $f_{np} = f - f'$, $g_{nn} = g_{pp} = g + g'$, and $g_{np} = g - g'$, dimensional normalization factor is usually taken to be $C_0 = \pi^2/[m_N p_F(\varrho_0)] \simeq 300 \text{ MeV} \cdot \text{fm}^3 \simeq 0.77 m_\pi^{-2}$, $D_{\pi^0}^R$ is the full retarded Green function of π^0 , $A_{\alpha\beta}$ is the corresponding NN^{-1} loop (without spin degeneracy factor 2)

$$A_{\alpha\beta} = \text{loop diagram}^{\beta}_{\alpha^{-1}}, \quad A_{nn}(\omega \simeq q) \simeq m_n^{*2}(4\pi^2)^{-1} \left(\ln \frac{1 + v_{Fn}}{1 - v_{Fn}} - 2v_{Fn} \right), \tag{6}$$

$A_{nn} \simeq -m_n^* p_{Fn}(2\pi^2)^{-1}$, for $\omega \ll qv_{Fn}$, $q \ll 2p_{Fn}$, and we for simplicity neglect proton hole contributions due to a small concentration of protons. Resummation of (1) in the charged channel yields

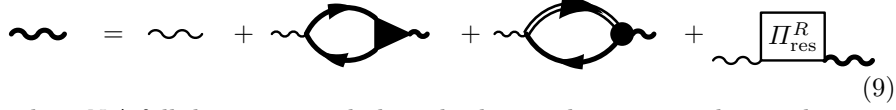
$$\begin{aligned}
\tilde{I}_{np}^R &= \text{diagram} = C_0 \left(\tilde{\mathcal{F}}_{np}^R + \tilde{\mathcal{Z}}_{np}^R \boldsymbol{\sigma}_1 \cdot \boldsymbol{\sigma}_2 \right) + f_{\pi N}^2 \tilde{\mathcal{T}}_{np}^R (\boldsymbol{\sigma}_1 \cdot \mathbf{k})(\boldsymbol{\sigma}_2 \cdot \mathbf{k}), \tag{7} \\
\tilde{\mathcal{F}}_{np}^R &= 2f'\tilde{\gamma}(f'), \quad \tilde{\mathcal{Z}}_{np}^R = 2g'\tilde{\gamma}(g'), \quad \tilde{\mathcal{T}}_{np}^R = \tilde{\gamma}^2(g')D_{\pi^-}^R, \\
\tilde{\gamma}^{-1}(x) &= 1 - 4xC_0A_{np}^R.
\end{aligned} \tag{8}$$

The LM parameters are rather unknown for isospin asymmetric nuclear matter and for $\varrho > \varrho_0$. Although some evaluations of these quantities have been done, much work is still needed to get convincing results. Therefore for estimates we will use the values extracted from atomic nucleus experiments. Using argumentation of a relative locality of these quantities we will suppose the LM parameters to be independent on the density for $\varrho > \varrho_0$. One then can expect that the most uncertain will be the value of the scalar constant f due to essential role of the medium-heavy σ meson in this channel. But this parameter does not enter the tensor force channel being most important in our case. Unfortunately, there are also essential uncertainties in numerical values of some of the LM parameters even for atomic nuclei. These uncertainties are, mainly, due to attempts to get the best fit of experimental data in each concrete case slightly modifying parameterization used for the residual part of the NN interaction. E.g., calculations [47] gave $f \simeq 0.25$, $f' \simeq 1$, $g \simeq 0.5$, $g' \simeq 1$ whereas [50–52], including QP renormalization pre-factors, derived the values $f \simeq 0$, $f' \simeq 0.5 \div 0.6$, $g \simeq 0.05 \pm 0.1$, $g' \simeq 1.1 \pm 0.1$.

Typical energies and momenta entering NN interaction of our interest are $\omega \simeq 0$ and $k \simeq p_{Fn}$. Then rough estimation yields $\gamma(g_{nn}, \omega \simeq 0, k \simeq p_{Fn}, \varrho = \varrho_0) \simeq 0.35 \div 0.45$. For $\omega = k \simeq T$ typical for the weak processes with participation of $\nu\bar{\nu}$ one has $\gamma^{-1}(g_{nn}, \omega \simeq k \simeq T, \varrho = \varrho_0) \simeq 0.8 \div 0.9$.

2.2 Virtual Pion Mode

Resummation of diagrams yields the following Dyson equation for pions



$$\text{wavy line} = \text{wavy line} + \text{loop with solid dot} + \text{loop with shaded dot} + \boxed{\Pi_{\text{res}}^R} \text{wavy line} \quad (9)$$

The $\pi N\Delta$ full-dot-vertex includes a background correction due to the presence of the higher resonances, Π_{res}^R is the residual retarded pion self-energy that includes the contribution of all the diagrams which are not presented explicitly in (9), as S wave πNN and $\pi\pi$ scatterings (included by double-wavy line in (2)). The full vertex takes into account NN correlations



$$\text{vertex with solid dot} = \text{vertex with wavy line} + \text{vertex with shaded circle} \quad (10)$$

Due to that the nucleon particle-hole part of Π_{π^0} is $\propto \gamma(g_{nn})$ and the nucleon particle-hole part of Π_{π^\pm} is $\propto \gamma(g')$. The value of the NN interaction in the pion channel is determined by the full pion propagator at small ω and $k \simeq p_{Fn}$, i.e. by the quantity $\tilde{\omega}^2(k) = -(D_\pi^R)^{-1}(\omega = 0, k, \mu_\pi)$. Typical momenta of our interest are $k \simeq p_{Fn}$. Indeed the momenta entering the NN interaction in MU and MMU processes are $k = p_{Fn}$, the momenta governing the MNB are $k = k_0$ [23] where the value $k = k_0 \simeq (0.9 \div 1)p_{Fn}$ corresponds to the minimum of $\tilde{\omega}^2(k)$. The quantity $\tilde{\omega} \equiv \tilde{\omega}(k_0)$ has the meaning of the *effective pion gap*. It is different for π^0 and for π^\pm since neutral and charged channels are characterized by different diagrams permitted by charge conservation, thus also depending on the value of the pion chemical potential, $\mu_{\pi^+} \neq \mu_{\pi^-} \neq 0$, $\mu_{\pi^0} = 0$. For $T \ll \varepsilon_{Fn}, \varepsilon_{Fp}$, $\mu_{\pi^-} = \mu_e = \varepsilon_{Fn} - \varepsilon_{Fp}$, as follows from equilibrium conditions for the reactions $n \rightarrow p\pi^-$ and $n \rightarrow pe\bar{\nu}$.

Change the sign of $\tilde{\omega}^2$ symbolizes the pion condensate phase transition. Typical density behaviour of $\tilde{\omega}^2$ is shown in Fig. 3. At $\varrho < (0.5 \div 0.7)\varrho_0$, one has $\tilde{\omega}^2 = m_\pi^2 - \mu_\pi^2$. For such densities the value $\tilde{\omega}^2(p_{Fn})$ essentially deviates from $m_\pi^2 - \mu_\pi^2$ tending to $m_\pi^2 + p_{Fn}^2 - \mu_\pi^2$ in small density limit.

At the critical point of the pion condensation ($\varrho = \varrho_{c\pi}$) the value $\tilde{\omega}^2$ with artificially switched off $\pi\pi$ fluctuations (dashed line in Fig. 3) changes its sign. In reality $\pi\pi$ fluctuations are significant in the vicinity of the critical point and there occurs the first-order phase transition to the inhomogeneous pion-condensate state [53–55]. Thereby there are two branches (solid curves in Fig. 3) with positive and respectively negative values for $\tilde{\omega}^2$. Calculations of [55] demonstrated that at $\varrho > \varrho_{c\pi}$ the free energy of the state with $\tilde{\omega}^2 > 0$, where the pion mean field is zero, becomes larger than that of the corresponding state with $\tilde{\omega}^2 < 0$ and a finite mean field. Therefore at $\varrho > \varrho_{c\pi}$ the state with $\tilde{\omega}^2 > 0$ is metastable and the state with $\tilde{\omega}^2 < 0$ and the pion mean field $\varphi_\pi \neq 0$ becomes the ground state.

The quantity $\tilde{\omega}^2$ demonstrates how much the virtual (particle-hole) mode with pion quantum numbers is softened at given density. The ratio $\alpha =$

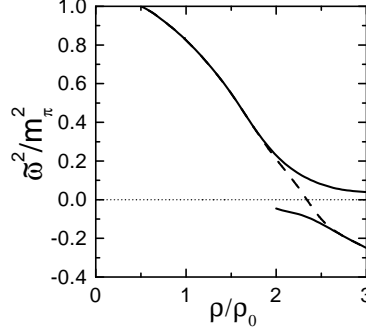


Fig. 3. Effective pion gap (for $\mu_{\pi 0} = 0$) versus baryon density, see [16].

$D_\pi[\text{med.}]/D_\pi[\text{vac.}] \simeq 6$ for $\varrho = \varrho_0$, $\omega = 0$, $k = p_{FN}$ and for isospin symmetric nuclear matter. However this essential so called “*pion softening*” [48] does not significantly enhance the NN scattering cross section due to a simultaneous essential suppression of the πNN vertex by NN correlations. Indeed, the ratio of the NN cross sections calculated with FOPE and MOPE is

$$R = \frac{\sigma[\text{FOPE}]}{\sigma[\text{MOPE}]} \simeq \frac{\gamma^4(g', \omega \simeq 0, k \simeq p_{FN})(m_\pi^2 + p_{FN}^2)^2}{\tilde{\omega}^4(p_{FN})}, \quad (11)$$

and for $\varrho = \varrho_0$ we have $R \lesssim 1$, whereas for $\varrho = 2\varrho_0$ we already get $R \sim 10$.

As follows from numerical estimates of different γ factors entering (4) and (7), the main contribution to NN interaction for $\varrho > \varrho_0$ is given by MOPE

$$\text{Thick bar} \simeq \text{Diagram with two nucleon lines and a wavy meson line} \quad (12)$$

whether this channel ($\mathcal{T} \propto (\boldsymbol{\sigma}_1 \cdot \mathbf{k})(\boldsymbol{\sigma}_2 \cdot \mathbf{k})$) of the reaction is not forbidden or suppressed by some specific reasons like symmetry, small momentum transfer, etc. The ϱ meson contribution to NN interaction is partially included in $g_{\alpha\beta}$, other part contributing to \mathcal{T} and $\tilde{\mathcal{T}}$ is minor ($\propto \tilde{\omega}^2/m_\varrho^2$). Thus instead of FOPE+ ϱ exchange, as the model of NN interaction which has been used in [6] in calculation of the emissivities of the two-nucleon reactions within the “*standard scenario*” of NS cooling one should use the full NN interaction given by (4) and (7) or, simplifying, approximated by its MOPE part.

2.3 Renormalization of the weak interaction.

The full weak coupling vertex that takes into account NN correlations is determined by (10) where now the wavy line should be replaced by the lepton pair. Thus for the vertex of our interest, $N_1 \rightarrow N_2 l \bar{\nu}$, we obtain [24,16]

$$V_\beta = \frac{G}{\sqrt{2}} [\tilde{\gamma}(f') l_0 - g_A \tilde{\gamma}(g') \mathbf{l} \boldsymbol{\sigma}], \quad (13)$$

for the β decay and

$$V_{nn} = -\frac{G}{2\sqrt{2}} [\gamma(f_{nn})l_0 - g_A\gamma(g_{nn})\mathbf{l}\boldsymbol{\sigma}], \quad V_{pp}^N = \frac{G}{2\sqrt{2}} [\kappa_{pp}l_0 - g_A\gamma_{pp}\mathbf{l}\boldsymbol{\sigma}] \quad (14)$$

$$\kappa_{pp} = c_V - 2f_{np}\gamma(f_{nn})C_0A_{nn}, \quad \gamma_{pp} = (1 - 4gC_0A_{nn})\gamma(g_{nn}), \quad (15)$$

for processes on the neutral currents $N_1N_2 \rightarrow N_1N_2\nu\bar{\nu}$, $V_{pp} = V_{pp}^N + V_{pp}^\gamma$, $G \simeq 1.17 \cdot 10^{-5} \text{ GeV}^{-2}$ is the Fermi weak coupling constant, $c_V = 1 - 4\sin^2\theta_W$, $\sin^2\theta_W \simeq 0.23$, $g_A \simeq 1.26$ is the axial-vector coupling constant, and $l_\mu = \bar{u}(q_1)\gamma_\mu(1-\gamma_5)u(q_2)$ is the lepton current. The tensor force contribution $\sim \mathbf{q}^2$ is small for typical $|\mathbf{q}| \simeq T$ or p_{Fe} , and for simplicity is omitted. Possibility of Brown-Rho scaling can be easily incorporated by scaling of g_A [56]. With a decrease of g_A^* the value $\varrho_{c\pi}$ increases. But it remains finite ($\simeq 2\varrho_0$ according to [57]) due to attractive contribution of the Δ isobar in (9), whereas one would expect $\varrho_{c\pi} \rightarrow \infty$ for $g_A^* \rightarrow 1$ ignoring Δ contribution.

The γ factors renormalize the corresponding vacuum vertices. These factors are essentially different for different processes involved. The matrix elements of the neutrino/antineutrino scattering processes $N\nu \rightarrow N\nu$ and of MNB behave differently in dependence on the energy-momentum transfer and whether $N = n$ or $N = p$ in the weak coupling vertex. Vertices

$$\begin{array}{c} \nu \\ \swarrow \quad \searrow \\ \text{---} \quad \text{---} \\ \nwarrow \quad \nearrow \\ N \end{array}, \quad \begin{array}{c} N \\ \swarrow \quad \searrow \\ \text{---} \quad \text{---} \\ \nwarrow \quad \nearrow \\ \nu \end{array} \quad (16)$$

are modified by the correlation factors (5) and (8). For $N = n$ these are $\gamma(g_{nn}, \omega, q)$ and $\gamma(f_{nn}, \omega, q)$ leading to an enhancement of the cross sections for $\omega > qv_{Fn}$ and to a suppression for $\omega < qv_{Fn}$. Renormalization of the proton vertex (vector part of $V_{pp}^N + V_{pp}^\gamma$) is governed by the processes [24,58]

$$\begin{array}{c} \nu \\ \swarrow \quad \searrow \\ \text{---} \quad \text{---} \\ \nwarrow \quad \nearrow \\ p \end{array} + \begin{array}{c} \nu \\ \swarrow \quad \searrow \\ \text{---} \quad \text{---} \\ \nwarrow \quad \nearrow \\ p \end{array} + \dots \quad (17)$$

being forbidden in vacuum. For the systems with $1S_0$ proton-proton pairing, $\propto g_A^2$ contribution to the squared matrix element (see (14)) is compensated by the corresponding contribution of the diagram with anomalous Green functions of protons. The vector current term is $\propto c_V^2$ in vacuum whereas it is $\propto \kappa_{pp}^2$ in medium (by first graph (17)). Thereby the corresponding vertices with participation of proton are enhanced in medium compared to the small vacuum value ($\propto c_V^2 \simeq 0.006$) leading to enhancement of the cross sections

(up to $\sim 10 \div 10^2$ times for $1.5 \div 3\rho_0$ depending on parameter choice). Also enhancement factor (up to $\sim 10^2$) comes from the intermediate in-medium photon (γ_m) whose propagator contains $1/m_\gamma^2 \sim 1/e^2$, where m_γ is the effective spectrum gap, that compensates small e^2 factor from electromagnetic vertices [58]. It is included by replacement $V_{pp}^N \rightarrow V_{pp}$. Other processes permitted in intermediate states like processes with pp^{-1} and with the pion are suppressed by a small proton density and by $q^2 \sim T^2$ pre-factors, respectively. First diagram (17) was considered in [24] where the pPBF process was suggested, and then in [16,26], and it was shown that nPBF and pPBF processes may give contributions of the same order of magnitude. Several subsequent papers overlooked these results and rediscovered the pPBF process ignoring the nucleon and the electron correlation effects. Specific contribution of second diagram for pPFB process was recently discussed in [59].

Paper [27] gives an other example demonstrating that although the vacuum branching ratio of a kaon decays is $\Gamma(K^- \rightarrow e^- + \nu_e)/\Gamma(K^- \rightarrow \mu^- + \nu_\mu) \approx 2.5 \times 10^{-5}$ in medium (due to Λp^{-1} decays of virtual K^-) it becomes to be of order of unit. Thus we see that in dependence of what reaction channel is considered in-medium effects may or strongly enhance the reaction rate under consideration or substantially suppress it.

2.4 Inconsistencies of FOPE model

Since FOPE model became the base of the "standard scenario" for cooling simulations we would like first to demonstrate principal inconsistencies of the model for the description of interactions in dense ($\rho \gtrsim \rho_0$) baryon medium. The only diagram in FOPE model which contributes to the MU and NB is

(18)

Dots symbolize FOPE. This is first available Born approximation diagram, i.e. second order perturbative contribution in $f_{\pi N}$. In order to be theoretically consistent one should use perturbation theory up to the very same second order in $f_{\pi N}$ for all the quantities. E.g., pion spectrum is then determined by pion polarization operator expanded up to the very same order in $f_{\pi N}$

$$\omega^2 \simeq m_\pi^2 + k^2 + \Pi_0^R(\omega, k, \rho), \quad \Pi_0^R(\omega, k, \rho) = \dots \text{ (diagram) } \dots \quad (19)$$

The value $\Pi^0(\omega, k, \rho)$ is easily calculated containing no any uncertain parameters. For $\omega \rightarrow 0$, $k \simeq p_F$ of our interest and for isospin symmetric matter

$$\Pi_0^R \simeq -\alpha_0 - i\beta_0\omega, \quad \alpha_0 \simeq \frac{2m_N p_F k^2 f_{\pi N}^2}{\pi^2} > 0, \quad \beta_0 \simeq \frac{m_N^2 k f_{\pi N}^2}{\pi} > 0. \quad (20)$$

Replacing this value to (19) we obtain a solution with $i\omega < 0$ already for $\varrho > 0.3\varrho_0$ that would mean appearance of the pion condensation. Indeed, the mean field begins to increase with the time passage $\varphi \sim \exp(-i\omega t) \sim \exp(\alpha t/\beta)$ until repulsive $\pi\pi$ interaction will not stop its growth. But it is experimentally proven that there is no pion condensation in atomic nuclei, i.e. even at $\varrho = \varrho_0$. The puzzle is solved as follows. FOPE model does not work for such densities. One should replace FOPE by the full NN interaction given by (4), (7). Essential part of this interaction is due to MOPE with vertices corrected by NN correlations. Also the NN^{-1} part of the pion polarization operator is corrected by NN correlations. Thus

$$\text{Diagram} \simeq \Pi_0^R(\omega, k, \varrho) \gamma(g', \omega, k, \varrho) \quad (21)$$

being suppressed by the factor $\gamma(g', \omega = 0, k \simeq p_F, \varrho \simeq \varrho_0) \simeq 0.35 \div 0.45$. Final solution of the dispersion relation (19), now with full Π instead of Π^0 , yields $i\omega > 0$ for $\varrho = \varrho_0$ whereas the solution with $i\omega < 0$, which shows the beginning of pion condensation, appears only for $\varrho > \varrho_{c\pi} > \varrho_0$.

3 Neutrino cooling of neutron stars

3.1 Emissivity of MMU process

Since DU process is forbidden up to sufficiently high density ϱ_{cU} , the main contribution for $\varrho < \varrho_{cU}$ and $T_{opac} > T > T_c$ comes from MMU processes schematically presented by two diagrams of Fig. 1. MNB reactions give smaller contribution [23]. For densities $\varrho \ll \varrho_0$ the main part of the NN interaction amplitude is given by the residual NN interaction. In this case the NN interaction amplitude can be better treated within the T matrix approach which sums up the ladder diagrams in the particle-particle channel rather than by LM parameters. Calculations of MNB processes with the vacuum T matrix [60] found essentially smaller emissivity than that given by FOPE. Also the in-medium modifications of the T matrix additionally suppress the rates of both MMU and MNB processes, see [61]. Thus even at small densities the FOPE model may give only a rough estimate of the emissivity of two nucleon processes. At $\varrho \gtrsim (0.5 \div 0.7) \varrho_0$ reactions in particle-hole channel and more specifically with participation of the soft pion mode begin to dominate.

Evaluations [23,42,43,16] showed that the dominating contribution to MMU rate comes from the second diagram of Fig. 1, namely from contributions to it given by the first two diagrams of the series

$$(22)$$

whereas the third diagram, which naturally generalizes the corresponding MU(FOPE) contribution, gives only a small correction for $\varrho \gtrsim \varrho_0$. The emissivity from the two first diagrams in a simplified notation [16,26] reads

$$\begin{aligned} \varepsilon^{MMU}[\text{MOPE}] &\simeq 2.4 \cdot 10^{24} T_9^8 \left(\frac{\varrho}{\varrho_0} \right)^{10/3} \frac{(m_n^*)^3 m_p^*}{m_N^4} \left[\frac{m_\pi}{\alpha \tilde{\omega}_{\pi^0}(p_{Fn})} \right]^4 \\ &\times \left[\frac{m_\pi}{\alpha \tilde{\omega}_{\pi^\pm}(p_{Fn})} \right]^4 \Gamma^8 F_1 \zeta(\Delta_n) \zeta(\Delta_p) \frac{\text{erg}}{\text{cm}^3 \text{ sec}}, \end{aligned} \quad (23)$$

where $T_9 = T/10^9$ K is the temperature, m_n^* and m_p^* are the nonrelativistic effective neutron and proton masses, and the correlation factor Γ^8 is roughly

$$\begin{aligned} \Gamma^8 &\simeq \gamma_\beta^2(\omega \simeq p_{Fe}, q \simeq p_{Fe}) \gamma^2(g_{nn}, \omega \simeq 0, k = p_{Fn}) \tilde{\gamma}^4(g', 0, p_{Fn}), \\ \gamma_\beta^2(\omega, q) &= \frac{\tilde{\gamma}^2(f', \omega, q) + 3g_A^2 \tilde{\gamma}^2(g', \omega, q)}{1 + 3g_A^2}, \end{aligned} \quad (24)$$

and the second term in the factor

$$F_1 \simeq 1 + \frac{3}{4\tilde{\gamma}^2(g', 0, p_{Fn}) \gamma_\beta^2(\omega \simeq p_{Fe}, q \simeq p_{Fe})} \left(\frac{\varrho}{\varrho_0} \right)^{2/3} \quad (25)$$

is the contribution of the pion decay from intermediate states (first diagram (22)). The quantity Γ effectively accounts for an appropriate product of the NN correlation factors in different $\pi N_1 N_2$ vertices. For charged pions the value $\mu_\pi \neq 0$ is incorporated in the expression for the effective pion gap, for neutral pions $\mu_\pi = 0$. The value $\alpha \sim 1$ depends on condensate structure, $\alpha = 1$ for $\varrho < \varrho_{c\pi}$, and $\alpha = \sqrt{2}$ taking account of the new excitations on the ground of the charged π condensate vacuum for $\varrho > \varrho_{c\pi}$. The factor

$$\zeta(\Delta_N) \simeq \begin{cases} \exp(-\Delta_N/T) & T \leq T_{cN}, \\ 1 & T > T_{cN}, \end{cases} \quad N = (n, p) \quad (26)$$

estimates the suppression caused by the nn and pp pairings. Deviation of these factors from simple exponents can be incorporated as in [35].

The ratio of the emissivities of MMU(MOPE) and MU(FOPE) is roughly

$$\frac{\varepsilon^{MMU}[\text{MOPE}]}{\varepsilon^{MU}[\text{FOPE}]} \simeq 10^3 \frac{\gamma^2(g_{nn}, 0, p_{Fn}) \tilde{\gamma}^2(g', 0, p_{Fn})}{\tilde{\omega}_{\pi^0}^4(p_{Fn}) \tilde{\omega}_{\pi^\pm}^4(p_{Fn})} (\varrho/\varrho_0)^{10/3}. \quad (27)$$

For $\varrho \simeq \varrho_0$ this ratio is ~ 10 whereas being estimated with the only third diagram (22) it would be less than unit.

3.2 Emissivity of DU-like processes

NPBF processes. The one-nucleon processes with neutral currents given by the second diagram (16) for $N = (n, p)$ are forbidden at $T > T_c$ by energy-momentum conservations but they can occur at $T < T_c$. Then physically the processes relate to NPBF, see Fig. 2. However they need special techniques to be calculated [33,24]. These processes $n \rightarrow n\nu\bar{\nu}$ and $p \rightarrow p\nu\bar{\nu}$ play very important role in the cooling of superfluid NS, see [24,25,16,26,36,35]. The emissivity for 3 types of neutrinos is given by [24,25]

$$\begin{aligned} \varepsilon[\text{nPBF}] &= \frac{3 \cdot 4G^2 (\xi_1 \gamma^2 (f_{nn}) + \xi_2 g_A^{*2} \gamma^2 (g_{nn})) p_{Fn} m_n^* \Delta_n^7}{15\pi^5} I\left(\frac{\Delta_n}{T}\right) \\ &\simeq \zeta \cdot 10^{28} \left(\frac{\varrho}{\varrho_0}\right)^{1/3} \frac{m_n^*}{m_N} \left(\frac{\Delta_n}{\text{MeV}}\right)^7 I\left(\frac{\Delta_n}{T}\right) \frac{\text{erg}}{\text{cm}^3 \cdot \text{sec}}, \quad T < T_{cn}, \quad (28) \end{aligned}$$

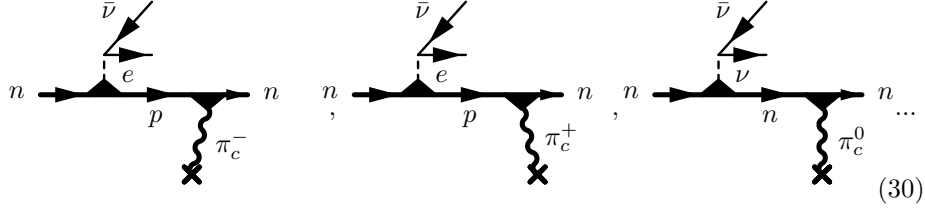
where $\xi_1 = 1$, $\xi_2 = 0$ for S -pairing and $\xi_1 = 2/3$, $\xi_2 = 4/3$ for P -pairing, compare [35]. I removed some misprints existed in [33,24,25,16]. For neutrinos $\omega(q) = q$ and correlations are not so essential as it would be for $\omega \ll q$. Taking $\gamma^2 \simeq 1.3$ in the range of S -pairing we get $\zeta \simeq 5$ whereas for the P -pairing with $g_A^* \simeq 1.1$ we obtain $\zeta \simeq 9$, in agreement with numerical evaluations [24] ($\zeta \simeq 7$) used then within the cooling code in [26], $I(x) = \int_0^\infty \text{ch}^5 y dy / (\exp(x \text{ch} y) + 1)^2$, $I(x \gg 1) \simeq \exp(-2\Delta/T) \sqrt{\pi T/4\Delta}$, that serves an appropriate asymptotic (28). Emissivity of the process $p \rightarrow p\nu\bar{\nu}$ is given by [24]

$$\varepsilon(\text{pPBF}) = \frac{12G^2 (\xi_1 \kappa_{pp}^2 + \xi_2 g_A^{*2} \gamma_{pp}^2 + \xi_3) p_{Fp} m_p^* \Delta_p^7}{15\pi^5} I\left(\frac{\Delta_p}{T}\right), \quad T < T_{cp} \quad (29)$$

and $\xi_2 = 0$ for protons paired in S -state in NS matter, $\xi_3 \lesssim 1$ is due to the second diagram (17) and has a complicated structure [58,59]. For the process (29) the part of NN and ee correlations is especially important. One has $\kappa_{pp}^2 \sim 0.05 \div 1$ for $1 \div 3\varrho_0$ and $\xi_3 \sim 1$, and $\kappa_{pp}^2 + \xi_3 \sim 1$ instead of a small $c_V^2 \simeq 0.006$ value in absence of correlations. Thereby, in agreement with [24,26,58,59], the emissivity of the process $p \rightarrow p\nu\bar{\nu}$ can be compatible with that for $n \rightarrow n\nu\bar{\nu}$ in dependence on the relation between Δ_p and Δ_n .

NPBF processes are very efficient for $T < T_c$ competing with MMU processes. The former win the content for not too massive stars. Analysis of above processes supports also our general conclusion on the crucial role of in-medium effects in the cooling scenario.

Pion (kaon) condensate processes. The P wave pion condensate can be of three types: π_s^+ , π^\pm , and π^0 with different values of the critical densities $\varrho_{c\pi} = (\varrho_{c\pi^\pm}, \varrho_{c\pi_s^+}, \varrho_{c\pi^0})$, see [48]. Thus above the threshold density for the pion condensation of the given type, the neutrino emissivity of the MMU process (23) is to be supplemented by the corresponding PU processes



The emissivity of the charged pion condensate processes with inclusion of the NN correlation effect (in a simplified treatment) renders, see [22,16],

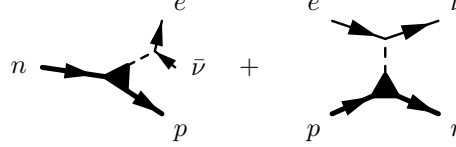
$$\varepsilon[\text{PU}] \simeq 7 \cdot 10^{26} \frac{p_{Fn}}{m_\pi} \frac{m_n^* m_p^*}{m_N^2} \gamma_\beta^2(p_{Fe}, p_{Fe}) \tilde{\gamma}^2(g', 0, p_{Fn}) T_9^6 \sin^2 \theta \frac{\text{erg}}{\text{cm}^3 \text{sec}} \quad (31)$$

Here $\varrho > \varrho_{c\pi}$ and $\sin \theta \simeq \sqrt{2|\tilde{\omega}^2|/m_\pi^2}$ for $\theta \ll 1$. Of the same order of magnitude are emissivities of other possible π condensate reactions, e.g. for $n\pi_c^0 \rightarrow npe\bar{\nu}$ process at $\theta \ll 1$ the numerical factor is about two times larger. Since π^\pm condensation probably reduces the energy gaps of the superfluid states by an order of magnitude, see [62], we may assume that superfluidity vanishes above $\varrho_{c\pi}$. Finally we note that though the PU processes have genuinely one-nucleon phase-space volumes, their contribution to the emissivity is suppressed relative to the DU by an additional $\tilde{\gamma}^2(g', 0, p_{Fn})$ suppression factor due to existence of the extra (πNN) vertex in the former case.

Fig. 4 compares the mass dependence of the neutrino cooling rates L_ν/C_V , L_ν is the neutrino luminosity, C_V is the heat capacity, for MMU(MOPE) and MU(FOPE) for non-superfluid matter. For the solid curves, the neutrino emissivity in pion-condensed matter is taken into account according to (31) and (23) with the parameter $\alpha = \sqrt{2}$. To be conservative we took $\varrho_{c\pi} \simeq 3\varrho_0$. Dashed curves correspond to the model where no pion condensation is allowed. As one sees, the medium polarization effects included in MMU may result in three order of magnitude increase of the cooling rate for the most massive stars. Even for stars of a rather low mass the cooling rate of MMU is still several times larger than for MU because even in this case the more efficient rate is given by the reactions shown by the right diagram in Fig. 1 (first two diagrams of (22)). The cooling rates for the NS of $M = 1.8M_\odot$ with and without pion condensate differ only moderately (by factor of 5 in this model). If we would take $\varrho_{c\pi}$ to be smaller the ratio of emissivity PU to MMU would decrease and could even become $\lesssim 1$ in the vicinity of $\varrho_{c\pi}$. Opposite, the reaction rates for the FOPE model are rather independent of the star's mass for the stars with masses below the critical value $1.63M_\odot$, at which transition into the pion condensed phase occurs, and then jump to the typical PU value. It is to be stressed that contrary to FOPE model, the MOPE model [23] consistently takes into account the pion softening effects for $\varrho < \varrho_{c\pi}$ and both the pion condensation and pion softening effects on the ground of the condensate for $\varrho > \varrho_{c\pi}$. For $\varrho > \varrho_{cK}$ the kaon condensate processes come into play. Most popular is the idea of the S wave K^- condensation (e.g. see [13]) which is allowed at $\mu_e > m_{K^-}^*$ due to possibility of the reaction $e \rightarrow K^- \nu$.

space volume ($q \sim T$) associated with zero sounds. Please also bear in mind an analogy of the processes (32) with the corresponding phonon processes in the crust.

DU processes. The proper DU processes in matter, as $n \rightarrow pe^- \bar{\nu}_e$ and $pe^- \rightarrow n\nu_e$,



$$(33)$$

should also be treated with the full vertices. They are forbidden up to the density ϱ_{cU} when triangle inequality $p_{Fn} < p_{Fp} + p_{Fe}$ begins to fulfill. For traditional EQS like that given by the variational theory [18] DU processes are permitted for $\varrho > 5\varrho_0$. The emissivity of the DU processes renders

$$\varepsilon^{DU} \simeq 1.2 \cdot 10^{27} \frac{m_n^* m_p^*}{m_N^2} \left(\frac{\mu_l}{100 \text{ MeV}} \right) \gamma_\beta^2 \min [\zeta(\Delta_n), \zeta(\Delta_p)] T_9^6 \frac{\text{erg}}{\text{cm}^3 \text{ sec}}, \quad (34)$$

where $\mu_l = \mu_e = \mu_\mu$ is the chemical potential of the leptons in MeV. In addition to the usually exploited result [15], (34) contains γ_β^2 pre-factor (13) due to NN correlations in the β decay vertices, see [24,26].

It was realized in [63] that the softening of the pion mode in dense neutron matter could also give rise to a rearrangement of single-fermion degrees of freedom due to violation of Pomeranchuk stability condition for $\varrho = \varrho_{cF} < \varrho_{c\pi}$. It may result in organization of an extra Fermi sea for $\varrho_{cF} < \varrho < \varrho_{c\pi}$ and at small momenta $p < 0.2p_{Fn}$, that in its turn opens a DU channel of neutrino cooling of NS from the corresponding layer. Due to the new feature of a temperature-dependent neutron effective mass, $m_n^* \propto 1/T$, we may anticipate extra essential enhancement of the DU process, corresponding to a reduction in the power of the temperature dependence from T^6 to T^5 . At early hot stage this layer becomes to be opaque for the neutrinos slowing the transport from the massive NS core to the exterior.

Basing on the Brown–Rho scaling idea [56], we argued in [64] for the charged ϱ meson condensation at a relevant density ($\varrho_{c\varrho} \sim 3\varrho_0$ if m_ϱ^* would decrease to that density up to $m_\varrho/2$). If happend, it would open DU reaction already for $\varrho < \varrho_{c\varrho}$ and close it for $\varrho > \varrho_{c\varrho}$ due to an essential modification of the nuclear asymmetry energy.

3.3 Comparison with soft X ray data

The heat transport within the crust establishes homogeneous density profile at times $\lesssim (1 \div 10)\text{yr}$. After that time the subsequent cooling is determined by simple relation $C_V \dot{T} = -L$, where $C_V = \sum_i C_{V,i}$ and $L = \sum_i L_i$ are sums of the partial contributions to the heat capacity (specific heat integrated over the volume) and the luminosity (emissivity integrated over the volume).

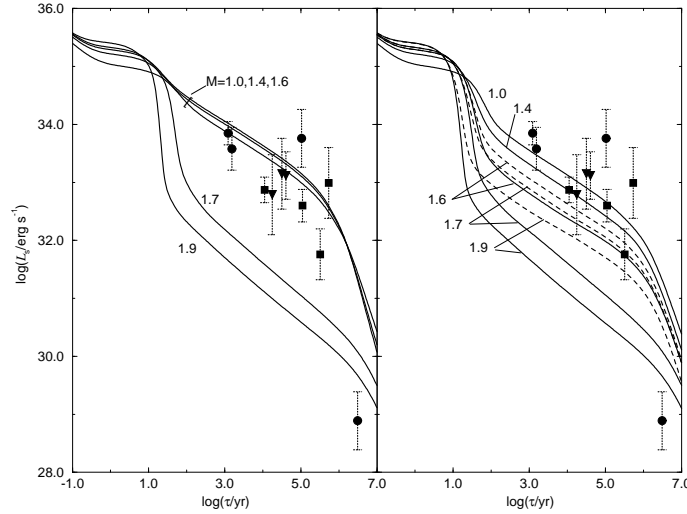


Fig. 5. Cooling of non-superfluid NS models of different masses constructed for the HV EOS [26]. Two graphs refer to cooling via MU(FOPE) +PU (left) and MMU(MOPE)+PU (right). In both cases, pion condensation is taken into account for the solid curves at $\varrho > \varrho_{c\pi}$, i.e. for $M > 1.6M_\odot$ ($\varrho_{c\pi}$ is chosen to be $3\varrho_0$). The dashed curves in the right graph refer to a somewhat larger value of $\tilde{\omega}^2(p_{Fn})$, without pion condensation. The observed luminosities are labeled by dots. Possibilities of Fermi sea rearrangement and ϱ^\pm condensation are ignored.

The nucleon pairing gaps are rather purely known. Therefore one may vary them. The "standard" and "nonstandard" scenarios of the cooling of NS of several selected masses for suppressed gaps are demonstrated in the left panel of Fig. 5, [26]. Depending on the star mass, the resulting photon luminosities are basically either too high or too low compared to those given by observations. Situation changes, if the MMU process (23) is included. Now, the cooling rates vary smoothly with the star mass (see right panel of Fig. 5) such that the gap between *standard* and *non-standard* cooling scenarios is washed out. More quantitatively, by means of varying the NS mass between $(1 \div 1.6) M_\odot$, one achieves an agreement with a large number of observed data points. This is true for a wide range of choices of the $\tilde{\omega}^2$ parameterization, independently whether pion (kaon) condensation can occur or not. Two parameterizations presented in Fig. 5 with pion condensation for $\varrho > 3\varrho_0$ and without it differ only in the range which is covered by the cooling curves. The only point which does not agree with the cooling curves belongs to the hottest pulsar PSR 1951+32. Other three points which according to Fig. 5, right panel, are also not fitted by the curves can be easily fitted by slight changes of the model parameters. The high luminosity of PSR 1951+32 may be due to internal heating processes, cf. [10].

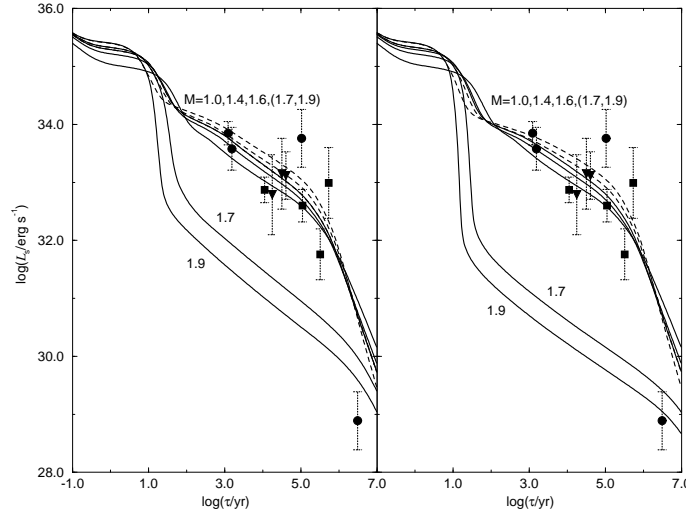


Fig. 6. Cooling of NS with different masses constructed for the HV EOS [26]. The cooling processes are MU-VS86, PU (only solid curves), NPBF, PPBF, and DU (only in the right graph). The dashed curves refer to the $M = 1.7$ and $1.9 M_\odot$ models without pion condensate. Possibilities of Fermi sea rearrangement and q^\pm condensation are ignored.

We turn now to cooling simulations where the MU, NPBF, DU and PU take place simultaneously. Parameters of the pairing gaps are from Fig. 6 of [26]. Fig. 6 shows the cooling tracks of stars of different masses, computed for the HV EQS. Very efficient at $T < T_c$ become to be NPBF processes which compete with MMU processes. The former prevail for not too massive stars in agreement with estimation [24]. The DU process is taken into account in the right graph, whereas it is neglected in the left graph. The solid curves refer again to the $\tilde{\omega}^2$ parameterization with phase transition to pion condensate, the dashed curves to the one without phase transition (see Fig. 4). For masses in the range between 1.0 and $1.6 M_\odot$, the cooling curves pass through most of the data points. We again recognize a photon luminosity drop by more than two orders of magnitude for the $1.7 M_\odot$ mass star with pion condensate, due to suppression of the pairing gaps in this case. This drop is even larger if the DU is taken into account (right graph). This allows to account for the photon luminosity of PSR 1929+10.

Thus, comparison with the observed luminosities shows that one gets quite good agreement between theory and observations if one includes into consideration all available in-medium effects assuming that the masses of the pulsars are different. We point out that the description of these effects is constructed in essentially the same manner for all the hadron systems as NS, atomic nuclei and heavy ion collisions, cf. [16,49].

3.4 Neutrino opacity

Important part of in-medium effects for description of neutrino transport at initial stage of NS cooling was discussed in [23,42,43,16], where correlation effects, pion softening and pion condensation, the latter for $\varrho > \varrho_{c\pi}$, were taken into account. The neutrino/antineutrino mean free paths can be evaluated from the corresponding kinetic equations via their widths $\Gamma_{\nu(\bar{\nu})} = -2\text{Im}\Pi_{\nu(\bar{\nu})}^R$, where Π^R is the retarded self-energy, or within the QPA for the nucleons they can be also estimated via the squared matrix elements of the corresponding reactions. Thereby the processes which the most efficiently contribute to the emissivity are at early times (for $T \gtrsim 1$ MeV) responsible for the opacity.

In the above "*nuclear medium cooling scenario*" at $T > T_c$ the most essential contribution was from MMU. Taking into account of NN correlations in the strong coupling vertices of two-nucleon processes like MMU and MNB suppresses the rates, whereas the softening of the pion propagator essentially enhances them. For rather massive NS MOPE wins the competition. The mean free path of neutrino/antineutrino in MMU processes is determined from the same diagrams (22) as the emissivity. Its calculation (see (23)) with the two first diagrams yields

$$\frac{\lambda_{\nu}^{MMU}}{R} \simeq \frac{1.5 \cdot 10^5}{F_1(2\Gamma)^8 T_9^4} \left(\frac{\varrho_0}{\varrho}\right)^{10/3} \frac{m_N^4}{(m_n^*)^3 m_p^*} \left[\frac{\alpha \tilde{\omega}_{\pi^0}(p_{Fn})}{m_{\pi}} \right]^4 \left[\frac{\alpha \tilde{\omega}_{\pi^{\pm}}(p_{Fn})}{m_{\pi}} \right]^4 \quad (35)$$

From the relation $\lambda_{\nu} \simeq R$ follows evaluation of T_{opac} . With the only first diagram we get a simple estimate

$$T_9^{opac} \simeq 11 \frac{\varrho_0}{\varrho} \frac{\tilde{\omega}^2(p_{Fn}^2)}{[4\gamma(g_{nn}, 0, p_{Fn})\tilde{\gamma}(g', 0, p_{Fn})]^{1/2}} \frac{m_N}{m_N^*}. \quad (36)$$

For averaged value of the density $\varrho \simeq \varrho_0$ corresponding to a medium-heavy NS ($< 1.4M_{\odot}$) with $\tilde{\omega}^2(p_{Fn}) \simeq 0.8m_{\pi}^2$, $\tilde{\gamma} \simeq \gamma \simeq (0.3 \div 0.4)$ we get $T_{opac} \simeq (1 \div 1.5)$ MeV that is smaller then the value $T_{opac} \simeq 2$ MeV estimated with FOPE [6]. For $\varrho \simeq 2\varrho_0$ that corresponds to a more massive NS we evaluate $T_{opac} \simeq (0.3 \div 0.5)$ MeV. Thus pion softening results in a substantial decrease of neutrino/antineutrino mean free paths and the value of T_{opac} .

The diffusion equation determines the characteristic time scale for the heat transport of neutrinos from the hot zone to the star surface $t_0 \sim R^2 C_V \sigma^{-1} T^{-3} / \lambda_{\nu}$ (σ is the Stefan-Boltzmann constant), whereas it follows that $t_0 \sim 10$ min. for $T \simeq 10$ MeV and $\varrho \simeq \varrho_0$, $\tilde{\omega}^2 \simeq 0.8m_{\pi}^2$, $\Gamma \simeq 0.4$, $m_N^*/m_N \simeq 0.9$, and t_0 becomes as large as several hours for $\varrho \simeq (2 \div 3)\varrho_0$. These estimates demonstrate that more massive NS cool down more slowly at $T > T_{opac}$ and faster at subsequent times then the less massive stars.

Due to in-medium effects neutrino scattering cross section on the neutrons shown by the first diagram (16) requires the NN correlation factor

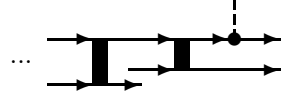
$$\gamma_{n\nu}^2(\omega, q) = \frac{\gamma^2(f_{nn}, \omega, q) + 3g_A^2 \gamma^2(g_{nn}, \omega, q)}{1 + 3g_A^2}, \quad (37)$$

as follows from (14). This results in a suppression of the cross sections for $\omega < qv_{Fn}$ and in an enhancement for $\omega > qv_{Fn}$. Neutrino scattering cross sections on the protons are modified by

$$\gamma_{p\nu}^2(\omega, q) = \frac{\kappa^2(f_{np}, f_{nn}, \omega, q) + 3g_A^2\gamma_{pp}^2(g_{nn}, \omega, q)}{1 + 3g_A^2}, \quad (38)$$

that results in the same order of magnitude correction as given by (37).

Also there is a suppression of the νN scattering and MNB reaction rates for soft neutrinos ($\omega \lesssim (3 \div 6)T$) due to multiple NN collisions

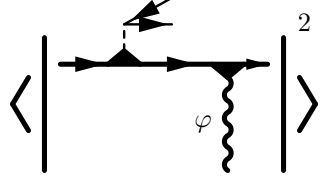

(39)

(LPM effect). One may estimate these effects simply multiplying squared matrix elements of the νN scattering and the MNB processes by the corresponding suppression pre-factors [28]. Qualitatively one may use a general pre-factor $C_0(\omega) = \omega^2/[\omega^2 + \Gamma_N^2]$, where Γ_N is the nucleon width and the ω is the energy of ν or $\nu\bar{\nu}$ pair. In some works, see [65,66], correction factor, like C_0 , was suggested at an ansatz level. Actually one does not need any ansatz reductions. OTF, see [28], allows to calculate the rates using the exact sum rule. The modification of the charged current processes due to LPM effect is unimportant since the corresponding value of ω is $\simeq p_{Fe} \gg \Gamma_N$.

The main physical result we discussed is that in medium the reaction rates are essentially modified. A suppression arises due to NN correlations (for $\omega \ll kv_{Fn}$) and infra-red pre-factors (coherence effects), and an enhancement due to the pion softening (and NN correlations for $\omega \sim q$) and due to opening up of new efficient reaction channels. The pion softening demonstrates that already for densities $\varrho < \varrho_0$ the nucleon system begins to feel that it may have π condensate phase transition for $\varrho > \varrho_{c\pi}$, although this $\varrho_{c\pi}$ value might be essentially larger than ϱ_0 or even not achieved.

4 The rate of radiation from dense medium. OTF

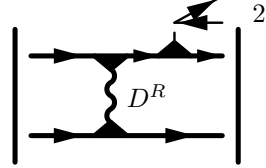
Perturbative diagrams are obviously irrelevant for calculation of in-medium processes and one should deal with dressed Green functions. The QPA for fermions is applicable if the fermion width is much less than all the typical energy scales essential in the problem ($\Gamma_F \ll \omega_{ch}$). In calculation of the emissivities of $\nu\bar{\nu}$ reactions the minimal scale is $\omega_{ch} \simeq 6T$, averaged $\nu\bar{\nu}$ energy for MNB reactions. For MMU $\omega_{ch} \simeq p_{Fe}$. For radiation of soft quanta of fixed energy $\omega < T$, $\omega_{ch} \simeq \omega$. Within the QPA for fermions, the reaction rate with participation of the fermion and the boson is given by [22,23]


(40)

For equilibrium ($T \neq 0$) system there is the exact relation

$$(\langle \hat{\varphi}_2^\dagger \hat{\varphi}_1 \rangle)(p) = iD^{-+} + |\varphi_c|^2 = \frac{A_B}{\exp(\frac{\omega}{T}) - 1} + |\varphi_c|^2, \quad A_B = -2\text{Im}D^R, \quad (41)$$

where $(\langle \hat{\varphi}_2^\dagger \hat{\varphi}_1 \rangle)(p)$ means the Fourier component of the corresponding non-equilibrium Green function and φ_c is the mean field. Thus the rate of the reaction is related to the boson spectral function A_B and the width (Γ_B) being determined by the corresponding Dyson equation, see (9). A_B is the delta-function at the spectrum branches related to resonance processes, like zero sound. The poles associated with the upper branches do not contribute at small temperatures due to a tiny thermal population of those branches. There is also a contribution to $\text{Im}D^R$ proportional to $\text{Im}I^R$ given by the particle-hole diagram. Within the QPA taking Im part means the cut of the diagram. Thus we show [23] that this contribution is the same as that could be calculated with the help of the squared matrix element of the two-nucleon process


(42)

This is precisely what one could expect using optical theorem. Thus unlimited series of all possible diagrams with in-medium Green functions (see (16), (30), (32), (33)) together with two-fermion diagrams (as given by (22)) and multiple-fermion diagrams (like (39)) would lead us to a double counting. The reason is that permitting the boson width effects (and beyond the QPA for fermions also permitting finite fermion widths) the difference between one-fermion, two-fermion and multiple-fermion processes in medium is smeared out. All the states are allowed and participate in production and absorption processes. Staying with the QP picture for fermions, the easiest way to avoid mentioned double counting is to calculate the reaction rates according to (40), i.e. with the help of the diagrams of the DU-like type, which already include all the contributions of the two-nucleon origin. Multiple NN collision processes should be added separately. On the other hand, it is rather inconvenient to explicitly treat all one-nucleon processes dealing with different specific quanta instead of using of the full NN interaction amplitude whenever it is possible. Besides, as we have mentioned, consideration of open fermion legs is only possible within the QPA for fermions since Feynman technique is not applicable if Green functions of ingoing and outgoing fermions have

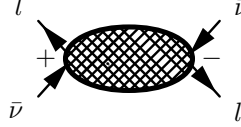
widths (that in another language means possibility of additional processes). Thus the idea came [24,28] to integrate over all in-medium states allowing all possible processes instead of specifying different special reaction channels.

In [24,28,27] it was shown that OTF in terms of full non-equilibrium Green functions is an efficient tool to calculate the reaction rates including finite particle widths and other in-medium effects. Applying this approach, e.g., to the antineutrino-lepton (electron, μ^- meson, or neutrino) production [24] we can express the transition probability in a direct reaction in terms of the evolution operator S ,

$$\frac{d\mathcal{W}_{X \rightarrow \bar{\nu}l}^{\text{tot}}}{dt} = \frac{(1 - n_l) dq_l^3 dq_{\bar{\nu}}^3}{(2\pi)^6 4 \omega_l \omega_{\bar{\nu}}} \sum_{\{X\}} \overline{\langle 0 | S^\dagger | \bar{\nu}l + X \rangle \langle \bar{\nu}l + X | S | 0 \rangle}, \quad (43)$$

where we presented explicitly the phase-space volume of $\bar{\nu}l$ states; lepton occupations of given spin, n_l , are put zero for ν and $\bar{\nu}$ which are supposed to be radiated directly from the system (for $T < T_{\text{opac}}$). The bar denotes statistical averaging. The summation goes over complete set of all possible intermediate states $\{X\}$ constrained by the energy-momentum conservation. It was also supposed that electrons/muons can be treated in the QPA, i.e. with zero widths. Then there is no need (although possible) to consider them in intermediate reaction states. Making use of the smallness of the weak coupling, we expand the evolution operator as $S \approx 1 - i \int_{-\infty}^{+\infty} T \{ V_W(x) S_{\text{nuc}}(x) \} dx_0$, where V_W is the Hamiltonian of the weak interaction in the interaction representation, S_{nuc} is the part of the S matrix corresponding to the nuclear interaction, and $T\{\dots\}$ is the chronological ordering operator. After substitution into (43) and averaging over the arbitrary non-equilibrium state of a nuclear system, there appear chronologically ordered (G^{--}), anti-chronologically ordered (G^{++}) and disordered (G^{+-} and G^{-+}) exact Green functions.

In graphical form the general expression for the probability of the lepton (electron, muon, neutrino) and anti-neutrino production is as follows



representing the sum of all closed diagrams ($-i\Pi^{-+}$) containing at least one $(-+)$ exact Green function. The latter quantity is especially important. Various contributions from $\{X\}$ can be classified according to the number N of G^{-+} lines in the diagram

$$\frac{d\mathcal{W}_{\bar{\nu}l}^{\text{tot}}}{dt} = \frac{(1 - n_l) d^3 q_{\bar{\nu}} d^3 q_l}{(2\pi)^6 4 \omega_{\bar{\nu}} \omega_l} \left(\begin{array}{c} l \\ + \quad \text{---} \quad \bar{\nu} \\ \bar{\nu} \quad \text{---} \quad l \end{array} \begin{array}{c} N=1 \\ \text{---} \end{array} \begin{array}{c} \bar{\nu} \quad l \\ + \quad \text{---} \quad \bar{\nu} \\ l \quad \text{---} \quad l \end{array} \begin{array}{c} N=2 \\ \text{---} \end{array} \dots \right) \quad (44)$$

This procedure suggested in [24] is actually very helpful especially if the

some simplified representations (e.g., as we used within Fermi liquid theory) the 4-point functions (blocks of NN interaction of given sign diagrams) behave like intermediate bosons (e.g. zero-sounds and dressed pions). In general it is not necessary to consider different quanta dealing instead with the full NN interaction (all diagrams of given sign). For particle propagation in an external field, e.g. infinitely heavy scattering centers (proper LPM effect), only the one-loop diagram remains, since one deals then with a genuine one-body problem. In the quasiclassical limit for fermions (with small occupations n_F) all the diagrams given by first line of series (46) with arbitrary number of " - + " lines are summed up leading to the diffusion result, for details see [28]. For small momenta q this leads to a suppression factor of the form $C = \omega^2/(\omega^2 + \Gamma_x^2)$, Γ_x incorporates rescattering processes. In general case the total radiation rate is obtained by summation of all diagrams in (46). The value $-i\Gamma^-+$ determines the gain term in the generalized kinetic equation for G^{-+} , see [67,68], that allows to use this method in non-equilibrium problems, like for description of neutrino transport in semi-transparent region of the neutrino-sphere of supernovae, as we may expect.

In the QP limit diagrams 1, 2, 4 and 5 of (46) correspond to the MMU and MNB processes related to a single in-medium scattering of two fermionic QP and can be symbolically expressed as Feynman amplitude (47a)



The one-loop diagram in (46) is particular, since its QP approximant in many cases vanishes as we have mentioned. However the full one-loop includes QP graphs of the type (47b), which survive to the same order in Γ_N/ω_{ch} as the other diagrams (therefore in [24] where QP picture was used this diagram was considered as allowed diagram). In QP series such a term is included in second diagram of (44) although beyond the QPA it is included as the proper self-energy insertion to the one-loop result, i.e. in first term (44) [28]. In fact it is positive definite and corresponds to the absolute square of the amplitude (47a). The other diagrams 2, 4 and 5 of (46) describe the interference of amplitude (47a) either with those amplitudes where the weak coupling quantum ($l\bar{\nu}$ pair) couples to another leg or with one of the exchange diagrams. For neutral interactions diagram (46:2) is more important than diagram 4 while this behavior reverses for charge exchange interactions (the latter is important, e.g., for gluon radiation from quarks in QCD transport due to color exchange interactions). Diagrams like 3 describe the interference terms due to further rescatterings of the source fermion with others as shown by (47c). Diagram (46:6) describes the production from intermediate states and relates to the Feynman graph (47d). For photons in the soft limit ($\omega \ll$

ε_F) this diagram (47d) gives a smaller contribution to the photon production rate than the diagram (47a), where the normal bremsstrahlung contribution diverges like $1/\omega$ compared to the $1/\varepsilon_F$ -value typical for the coupling to intermediate fermion lines. For $\nu\bar{\nu}$ bremsstrahlung (47d) gives zero due to symmetry. However in some cases the process (47d) might be very important even in the soft limit. This is indeed the case for the MMU process considered above. Some of the diagrams which are not presented explicitly in (46) give more than two pieces, if being cut, so they never reduce to the Feynman amplitudes. However in the QPA they give zero contribution [28].

With $\Gamma_F \sim \pi^2 T^2 / \varepsilon_F$ for Fermi liquids, the criterion $\Gamma_F \ll \omega_{ch} \sim T$ is satisfied for all thermal excitations $\Delta\varepsilon \sim T \ll \varepsilon_F / \pi^2$. However with the application to soft radiation this concept is no longer justified. Indeed series of QP diagrams is not convergent in the soft limit and there is no hope to ever recover a reliable result by a finite number of QP diagrams for the production of soft quanta. With *full Green functions*, however, one obtains a description that uniformly covers both the soft ($\omega \ll \Gamma_F$) and the hard ($\omega \gg \Gamma_F$) regimes. In the vicinity of $\varrho_{c\pi}$ the quantity Γ_F being roughly estimated in [53,55] as $\Gamma_F \propto \pi^2 \Gamma^2 T m_\pi / \bar{\omega}$, and coherence effects come into play.

In order to correct QP evaluations of different diagrams by the fermion width effects for soft radiating quanta one can simply multiply the QP results by different pre-factors [28]. E.g., comparing the one-loop result at non-zero Γ_F with the first non-zero diagram in the QPA ($\Gamma_F = 0$ in the fermion Green functions) we get

$$\begin{array}{c} + \\ \bullet \end{array} \text{---} \text{---} \text{---} \begin{array}{c} - \\ \bullet \end{array} \text{---} \text{---} \text{---} = C_0(\omega) \left\{ \begin{array}{c} + \\ \bullet \end{array} \text{---} \text{---} \text{---} \begin{array}{c} - \\ \bullet \end{array} \text{---} \text{---} \text{---} \right\}_{\text{QPA}}, \quad (48)$$

at small momentum q . For the next order diagrams we have

$$\begin{array}{c} + \\ \bullet \end{array} \text{---} \text{---} \text{---} \begin{array}{c} - \\ \bullet \end{array} \text{---} \text{---} \text{---} = C_1(\omega) \left\{ \begin{array}{c} + \\ \bullet \end{array} \text{---} \text{---} \text{---} \begin{array}{c} - \\ \bullet \end{array} \text{---} \text{---} \text{---} \right\}_{\text{QPA}}, \quad C_1(\omega) = \omega^2 \frac{\omega^2 - \Gamma_F^2}{(\omega^2 + \Gamma_F^2)^2},$$

$$\begin{array}{c} + \\ \bullet \end{array} \text{---} \text{---} \text{---} \begin{array}{c} - \\ \bullet \end{array} \text{---} \text{---} \text{---} = C_0(\omega) \left\{ \begin{array}{c} + \\ \bullet \end{array} \text{---} \text{---} \text{---} \begin{array}{c} - \\ \bullet \end{array} \text{---} \text{---} \text{---} \right\}_{\text{QPA}}, \quad C_0(\omega) = \frac{\omega^2}{\omega^2 + \Gamma_F^2}. \quad (49)$$

where factors C_0, C_1, \dots cure the defect of the QPA for soft ω . The factor C_0 complies with the replacement $\omega \rightarrow \omega + i\Gamma_F$. A similar factor is observed in the diffusion result, where however the macroscopic relaxation rate Γ_x enters, due to the resummation of all rescattering processes.

Finally, we demonstrated how to calculate the rates of different reactions in dense equilibrium and non-equilibrium matter and compared the results

derived in closed diagram technique with those obtained in the standard technique of computing of the squared matrix elements.

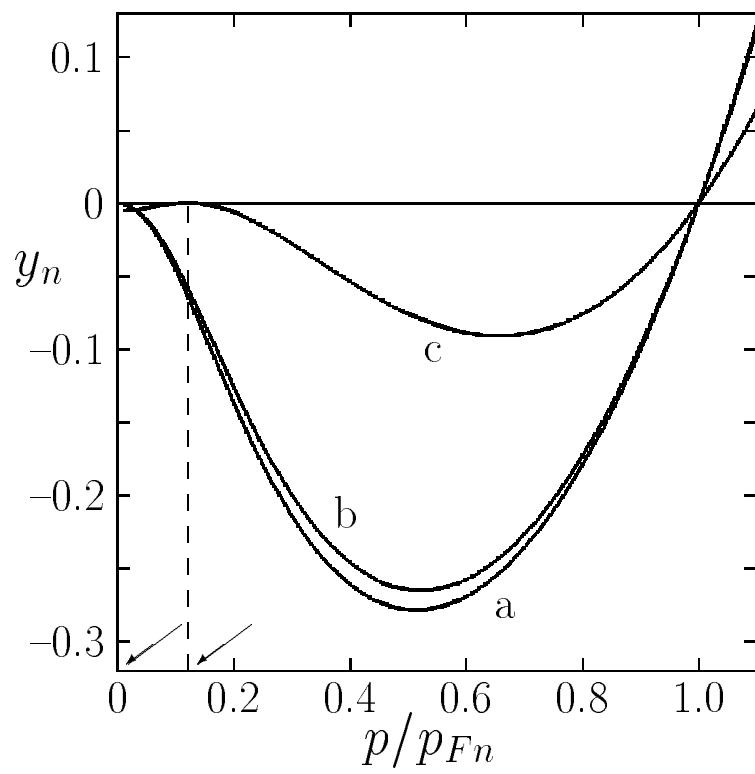
Concluding, the "*nuclear medium cooling scenario*" allows easily to achieve agreement with existing data. However there remains essential uncertainty in quantitative predictions due to a pure knowledge, especially, of the residual interaction treated above in an economical way within a phenomenological Fermi liquid model which needs further essential improvements.

Acknowledgement: Author appreciates the hospitality and support of GSI Darmstadt and ECT* Trento. He thanks E. Kolomeitsev for discussions.

References

1. S. Shapiro, S.A. Teukolsky: *Black Holes, White Dwarfs and Neutron Stars: The Physics of Compact Objects.* (Wiley, New York 1983), chapter 11
2. D. Pines, R. Tamagaki, S. Tsuruta (eds.): *Neutron Stars.* (Addison-Weseley, New York 1992)
3. Ed. by M. A. Alpar, Ü. Kiziloglu, J. van Paradijs (eds.): *The Lives of the Neutron Stars* (NATO ASI Ser. C, 450; Dordrecht: Kluwer 1995)
4. J.N. Bahcall, R.A. Wolf: Phys. Rev. B **140**, 1445 (1965)
5. S. Tsuruta, A.G.W. Cameron: Canad. J. Phys. **43**, 2056 (1965)
6. B. Friman, O.V. Maxwell: Ap. J. **232**, 541 (1979)
7. O.V. Maxwell: Ap. J. **231**, 201 (1979)
8. S. Tsuruta: Phys. Rep. **56**, 237 (1979)
9. K. Nomoto, S. Tsuruta: Ap. J. Lett. **250**, 19 (1981)
10. Ch. Schaab, F.Weber, M.K. Weigel, N.K. Glendenning: Nucl. Phys. A **605**, 531 (1996)
11. G. Flowers, P.G. Sutherland, J.R. Bond: Phys. Rev. D **12**, 315 (1975)
12. O. Maxwell, G.E. Brown et al.: Ap. J. **216**, 77 (1977)
13. G.E. Brown, K. Kubodera, D. Page, P. Pizzochero: Phys. Rev. D **37**, 2042 (1988)
14. T. Tatsumi: Prog. Theor. Phys. **88**, 22 (1988)
15. J.M. Lattimer, C.J. Pethick, M. Prakash, P. Haensel: Phys. Rev. Lett. **66**, 2701 (1991)
16. A.B. Migdal, E.E. Saperstein, M.A. Troitsky, D.N. Voskresensky: Phys. Rep. **192**, 179 (1990)
17. T. Takatsuka, R. Tamagaki: Prog. Theor. Phys. **97**, 1 (1997)
18. A. Akmal, V.R. Pandharipande, D.G. Ravenhall: Phys. Rev. C **58**, 1804 (1998)
19. T. Suzuki, H. Sakai, T. Tatsumi, nucl-th/9901097
20. G.E. Brown, C.H. Lee, M. Rho, V. Thorsson: Nucl. Phys. A **567**, 937 (1994)
21. E.E. Kolomeitsev, D.N. Voskresensky, B. Kämpfer: Nucl. Phys. A **588**, 889 (1995)
22. D.N. Voskresensky, A.V. Senatorov: JETP Lett. **40**, 1212 (1984)
23. D.N. Voskresensky, A.V. Senatorov: JETP **63**, 885 (1986)
24. D.N. Voskresensky, A.V. Senatorov: Sov. J. Nucl. Phys. **45**, 411 (1987)
25. A.V. Senatorov, D.N. Voskresensky: Phys. Lett. B **184**, 119 (1987)
26. Ch. Schaab, D. Voskresensky, et al.: Astron. Astrophys. **321**, 591 (1997)
27. E.E. Kolomeitsev, D.N. Voskresensky: Phys. Rev. C **60**, 034610 (1999)

28. J. Knoll, D. N. Voskresensky: Phys. Lett. B **351**, 43 (1995); Ann. Phys. (New York) **249**, 532 (1996)
29. N.K. Glendenning: Phys. Rev. D **46**, 1274 (1992)
30. M.B. Christiansen, N.K. Glendenning: astro-ph/0008207
31. T. Tatsumi: Prog. Theor. Phys. **69**, 1137 (1983)
32. H. Umeda, K. Nomoto, et al: Ap.J. **431**, 309 (1994)
33. E. Flowers, M. Ruderman, P. Sutherland: Ap. J. **205**, 541 (1976)
34. D.G. Yakovlev, A.D. Kaminker, K.P. Levenfish: Astron. Astrophys. **343**, 650 (1999)
35. D.G. Yakovlev, K.P. Levenfish, Yu.A. Shibarov: Phys. Usp. **42**, 737 (1999)
36. D. Page: *Many Faces of Neutron Stars*, ed. by R. Buccheri, J. van Paradijs, M.A. Alpar (Dordrecht, Kluwer, 1998) p. 538
37. R.F. Sawyer, A. Soni: Ap. J. **230**, 859 (1979)
38. R.F. Sawyer: Ap. J. **237**, 187 (1980)
39. R.F. Sawyer, A. Soni: Ap. J. **216**, 73 (1977)
40. S. Reddy, M. Prakash: Ap.J. **423**, 689 (1997)
41. J.A. Pons, S. Reddy, et al.: Ap.J. **513**, 780 (1999)
42. D.N. Voskresensky, A.V. Senatorov, B. Kämpfer, H. Haubold: Astrophys. Space Sci. **138**, 421 (1987)
43. H. Haubold, B. Kämpfer, A.V. Senatorov, D.N. Voskresensky: Astron. Astrophys. **191**, L22 (1988)
44. A. Sedrakian, A. Dieperink: Phys. Lett. B **463**, 145 (1999); nucl-th/0005029
45. S. Yamada: Nucl. Phys. A **662**, 219 (2000)
46. L.D. Landau: Sov. JETP. **3**, 920 (1956)
47. A.B. Migdal: *Theory of Finite Fermi Systems and Properties of Atomic Nuclei* (Willey and Sons, New York 1967; second. ed. (in Rus.), Nauka, Moscow, 1983)
48. A.B. Migdal: Rev. Mod. Phys. **50**, 107 (1978)
49. D. N. Voskresensky: Nucl. Phys. A **555**, 293 (1993)
50. E.E. Saperstein, S.V. Tolokonnikov: JETP Lett. **68**, 553 (1998)
51. S.A. Fayans, D. Zawischa: Phys. Lett. B **363**, 12 (1995)
52. I.N. Borzov, S.V. Tolokonnikov, S.A. Fayans: Sov. J. Nucl. Phys. **40**, 732 (1984)
53. A.M. Dyugaev: Pisma v ZhETF. **22**, 181 (1975)
54. D.N. Voskresensky, I.N. Mishustin: JETP Lett. **34**, 303 (1981); Sov. J. Nucl. Phys. **35**, 667 (1982)
55. A.M. Dyugaev: ZhETF. **83**, 1005 (1982); Sov. J. Nucl. Phys. **38**, 680 (1983)
56. G.E. Brown, M. Rho: Phys. Rev. Lett. **66**, 2720 (1991); Phys. Rep. **269**, 333 (1996)
57. G. Baym, D. Campbell, R. Dashen, J. Manassah: Phys. Lett. B **58**, 304 (1975)
58. D.N. Voskresensky, E.E. Kolomeitsev, B. Kämpfer: JETP. **87**, 211 (1998)
59. L.B. Leinson: Phys. Lett. B **473**, 318 (2000)
60. C. Hanhart, D. R. Phillips, S. Reddy: nucl-th/0003445
61. D. Blaschke, G. Röpke, et al.: MNRAS. **273**, 596 (1995)
62. T. Takatsuka, R. Tamagaki: Progr. Theor. Phys. **64**, 2270 (1980)
63. D.N. Voskresensky, V. A. Khodel, M. V. Zverev, J.W. Clark: Ap. J. Lett. **533**, 127 (2000)
64. D.N. Voskresensky: Phys. Lett. B **392**, 262 (1997)
65. G. Raffelt, D. Seckel: Phys. Rev. D **52**, 1780 (1995)
66. S. Hannestad, G. Raffelt: astro-ph/971132
67. Yu.B. Ivanov, J. Knoll, D.N. Voskresensky: Nucl. Phys. A **672**, 314 (2000)
68. Yu.B. Ivanov, J. Knoll, H.van Hees, D.N. Voskresensky: nucl-th/0005075



Medium Effects in Neutrino Cooling of Neutron Stars

Dmitri N. Voskresensky¹

*Moscow Institute for Physics and Engineering, Russia, 115409 Moscow,
Kashirskoe shosse 31,
Gesellschaft für Schwerionenforschung GSI
P.O.Box 110552, D-64220 Darmstadt, Germany*

Abstract

This review demonstrates that neutrino emission from the dense hadronic component in neutron stars is subject of strong modifications due to collective effects in the nuclear matter. With the most important in-medium processes incorporated in the cooling code an overall agreement with available soft X ray data can be easily achieved. With these findings so called "*standard*" and "*non-standard*" cooling scenarios are replaced by one general "*nuclear medium cooling scenario*" which relates slow and rapid neutron star coolings to the star masses (interior densities). In-medium effects take important part also at early hot stage of neutron star evolution decreasing the neutrino opacity for less massive and increasing for more massive neutron stars leading to a delay of the neutrino puls in the later case. An adequate formalism for calculation of neutrino radiation from strongly coupled matter is presented that treats on equal footing one-nucleon and multiple-nucleon processes as well as resonance boson contributions.

1 Introduction

The EINSTEIN, EXOSAT and ROSAT observatories have measured surface temperatures of certain neutron stars and put upper limits on the surface temperatures of some other neutron stars (cf. [1–3] and further references therein). The data for some supernova remnants indicate rather slow cooling, while the data for several pulsars point to an essentially more rapid cooling.

The physics of neutron star cooling is based on a number of ingredients, among which the neutrino emissivity of the high-density hadronic matter in the star's core plays a crucial role. Neutron star temperatures are such that, except first seconds–hours,

¹ Electronic mail: D.Voskresensky@gsi.de

neutrinos/antineutrinos radiate energy directly from the star without subsequent collisions, since $\lambda_\nu, \lambda_{\bar{\nu}} \gg R$, where $\lambda_\nu, \lambda_{\bar{\nu}}$ are the neutrino and antineutrino mean free paths and R is star's radius. In the so called "*standard scenario*" of the neutron star cooling (scenario for slow cooling) the most important channel up to temperatures $T \leq (10^8 - 10^9)\text{K}$ belongs to the modified Urca (MU) process $nn \rightarrow npe\bar{\nu}$. First estimates of its emissivity were done in refs [4,5]. Friman and Maxwell in refs. [6,7] recalculated the emissivity of this process in the model, where the nucleon-nucleon interaction was treated with the help of slightly modified free one-pion exchange (FOPE). Their important result for the emissivity, $\varepsilon_\nu[\text{FOPE}]$, was proved to be by an order of magnitude larger than the previously obtained one. Namely the value $\varepsilon_\nu[\text{FOPE}]$ was used in various computer simulations resulting in the "*standard scenario*" of the cooling, e.g. cf. refs [8–10]. Besides the MU process, in the framework of the "*standard scenario*" numerical codes included also processes of the nucleon (neutron and proton) bremsstrahlung (NB) $nn \rightarrow nn\nu\bar{\nu}$ and $np \rightarrow np\nu\bar{\nu}$, which lead to a smaller contribution to the emissivity than the MU, cf. refs [11,6]. Medium effects enter the above two-nucleon (MU and NB) rates mainly through the effective mass of the nucleons which has a smooth density dependence. Therefore within FOPE model the density dependence of the rates is rather weak and the neutrino radiation from a neutron star depends only very weakly on its mass. This is the reason why the "*standard scenario*" based on the result of [6], though complying well with several slowly cooling pulsars, fails to explain the data of the more rapidly cooling ones. Also "*standard scenario*" included processes contributing to the emissivity in the neutron star crust which become to be important at a lower temperature.

The *non-standard scenario* included so called exotics, associated with different types of direct Urca-like processes, i.e. the pion Urca (PU) [12] and kaon Urca (KU) [13,14] β -decay processes and direct Urca (DU) on nucleons and hyperons [15] possible only in sufficiently dense interiors of rather massive neutron stars. The main difference in the cooling efficiency driven by the DU-like processes on one hand and the MU and NB processes on the other hand lies in the rather different phase spaces associated with these reactions. In the MU and NB case the available phase space is that of a two-fermion origin, while in the pion (kaon) β -decay and DU on nucleons and hyperons it is that of a one-fermion origin. Critical density of pion condensation in neutron star matter is $\rho_{c\pi} \simeq (1 - 3)\rho_0$ depending on the type of condensation (neutral or charged) and the model, see [16–19]. Critical density of kaon condensation is $\rho_{cK} \simeq (2 - 6)\rho_0$ depending on the type (K^- or \bar{K}^0 , S or P wave) and the model, see [20,69]. Critical density for the DU process is $\rho_{cU} \simeq (3 - 6)\rho_0$ depending on the model for the equation of state, see [15,18]. Most recent calculations [19] estimated critical density of neutral pion condensation as $2.5\rho_0$ and for the charged one as $1.7\rho_0$, whereas variational calculations [18] argued even for smaller critical densities ($\simeq 1.3\rho_0$ for neutral pion condensation). On the other hand the equation of state of ref. [18] allows for DU process only at $\rho > 5\rho_0$.

There is no bridge between "*standard*" and "*non-standard*" scenarios due to complete ignorance of in-medium modifications of NN interaction which allows for strong polarization of the soft modes (like virtual dressed pion and kaon modes serving

a part of in-medium baryon–baryon interaction). Only due to increase of such a polarization with the baryon density mentioned condensates may appear and it seems thereby quite inconsistent to ignore these softening effects, i.e. precursors of the condensations for $\rho < \rho_{c\pi}$, and suddenly switch on the condensates for $\rho > \rho_{c\pi}$.

Now let us basing on the results [22–25,16,26] briefly discuss a general “*nuclear medium cooling scenario*” which treats obvious caveats of two mentioned above scenarios. First of all one observes that in the nuclear matter many new reaction channels are opened up compared to the vacuum processes, see [22]. Generally speaking, standard Feynman technique fails to calculate in-medium reaction rates if the particle widths are important since there are no free particle asymptotic states in matter. Then summation of all perturbative Feynman diagrams where free Green functions are replaced by the in-medium ones leads to a double counting due to multiple repetitions of some processes (for an extensive discussion of this defect see [27]). This calls a formalism dealing with closed diagrams (integrated over all possible in-medium particle states) with full non-equilibrium Green functions. Such a formalism was elaborated in [24] within quasiparticle approximation for nucleons and was called “*optic theorem formalism (OTF) in non-equilibrium diagram technique*”. It was demonstrated that both standard calculation of the rates via squared reaction matrix elements and calculation using OTF coincide within quasiparticle approximation picture for the fermions. In [28] the formalism was generalized to include arbitrary particle widths effects. The latter formalism treats on equal footing one-nucleon and multiple-nucleon processes as well as resonance reaction contributions of the boson origin, as processes with participation of zero-sounds and reactions on the boson condensates. Each diagram in the series with full Green functions is free from the infrared divergences. Both, the correct quasiparticle and quasiclassical limits are recovered.

Except for very early stage of neutron star evolution (seconds - hours) typical averaged lepton energy ($\gtrsim T$) is larger then the nucleon particle width $\Gamma_N \sim T^2/\epsilon_{FN}$ and the nucleons can be treated within the quasiparticle approximation. This observation much simplifies the consideration since one can use an intuitive way of separation of the processes according to the available phase space. The one-nucleon processes have the largest emissivity (if they are not forbidden by energy-momentum conservations), then two-nucleon processes come into play, etc.

In the temperature interval $T_c < T < T_{opac}$ (T_c is typical temperature for the nucleon pairing and T_{opac} is typical temperature at which neutrino/antineutrino mean free path $\lambda_\nu/\lambda_{\bar{\nu}}$ becomes to be of the order of the star radius R) the neutrino emission is dominated by the medium modified Urca (MMU) and medium nucleon bremsstrahlung (MNB) processes since one-nucleon processes like DU, PU and KU, are forbidden up to sufficiently large nucleon density. Corresponding diagrams of MMU and MNB are schematically shown in Fig. 1. Refs [22–25,16] considered NN interaction within Fermi liquid Landau–Migdal approach. They incorporated the softening of the medium one–pion exchange (MOPE) mode, other medium polarization effects, like nucleon-nucleon correlations in the vertices, renormalization of the

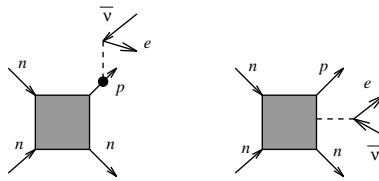


Fig. 1. Antineutrino emission from a nucleon leg (left graph) and from intermediate scattering states (right). Full dot includes weak coupling vertex renormalization.

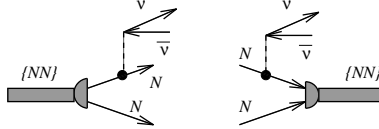


Fig. 2. Neutrino-antineutrino emission from Cooper pair-breaking (left graph) and pair-formation processes (right graph).

local part of NN interaction by the loops, as well as the possibility of the neutrino emission from the intermediate reaction states and resonance DU-like reactions going on zero sounds and the boson condensates. Refs [23,25,16] have demonstrated that for $\rho \gtrsim \rho_0$ second diagram of Fig. 1 gives the main contribution to the emissivity of MMU process rather than the first one which contribution has been evaluated much earlier in the framework of FOPE model in ref. [6]. This fact essentially modifies the absolute value as well as the density dependence of the $nn \rightarrow npe\bar{\nu}$ process rate which becomes to be very sharp. Thereby, for stars of masses larger than the solar mass the resulting emissivities were proved to be substantially larger than those values calculated in FOPE model. With increase of the star mass (central density) pion mode continues to soften and MMU and MNB rates still increase. At $\rho > \rho_{c\pi}$ pion condensation begins to contribute. Actually, the condensate droplets exist already at a smaller density in the mixed phase appearing in systems having more than one conserved charge [29,30]. At $T > T_{melt}$, where T_{melt} is the melting temperature, roughly \sim several MeV, the mixed phase is in liquid state and PU processes on independent condensate droplets are possible. At $T < T_{melt}$ condensate droplets are placed in a crystalline lattice that substantially suppresses corresponding neutrino processes.

Ref. [12] considered the reaction channel $n \rightarrow p\pi_c^- e\bar{\nu}$, whereas refs [22,23] included other possible pion π^+ , π^\pm , π^0 condensate processes with charged and neutral currents (e.g., like $n\pi_c^+ \rightarrow p\nu\bar{\nu}$ and $n\pi_c^0 \rightarrow n\nu\bar{\nu}$) as well as analogous resonance reactions going on zero sounds which are also possible at $\rho < \rho_{c\pi}$. Due to NN correlations all pion condensate rates are significantly suppressed (by factors $\sim 10 - 100$ compared to first estimate [12], see [31,22,23]. At $\rho \sim \rho_{c\pi}$ both MMU and PU processes are of the same order of magnitude showing a smooth transition to higher densities (star masses) in the "nuclear medium cooling scenario" being absent in the "standard" and "non-standard" scenarios.

For $T < T_c$ the reactions of neutrino pair radiation from superfluid nucleon pair breaking and formation (NPBF) shown in Fig. 2 become to be dominant processes. The neutron pair breaking and formation (nPBF) process for the case of the neutron

$1S_0$ pairing was first calculated in ref. [32] using standard Bogolyubov technique. Later this process was independently calculated in [24,25] as demonstration of efficiency of OTF within the closed non-equilibrium diagram technique developed there. Moreover ref. [24] calculated emissivity of the corresponding process on proton (pPFB) taking into account strong coupling $p\nu\bar{\nu}$ vertex renormalization (see first diagram eq. (20) below). It resulted in a hundred times enhancement in the medium of pPFB emissivity compared to that estimated with the vacuum vertex, leading to that both nPFB and pPFB emissivities were proved to be of the same order of magnitude. Emissivities of NPBF processes have the same suppression factor $\sim \exp(-2\Delta/T)$ as MU, NB, MMU and MNB processes at $T < T_c$ but compared to the latter the NPBF processes have a large one nucleon phase space volume. Ref. [35] included peculiarities of $3P_2$ pairing. In the $3P_2(|m_J|=2)$ case, where m_J is projection of the total pair momentum onto quantization axis, exponential suppression of specific heat and the emissivity is replaced by only a power law suppression since the gap vanishes at the Fermi sphere poles, as was first claimed in ref. [24] and then included in refs [36,33] which overlooked this more earlier suggestion.

At this instance I would like to do a historic remark relating to estimation of the NPBF processes since in some refs (see [34,33]) was expressed a surprise why these processes were not on a market during many years. First work [32], although found correct analytic expression for $1S_0$ pairing of neutrons, numerically underestimated the emissivity by more than an order of magnitude (by factors 20 and 50 for S and P pairing cases respectively). Also there was no statement on the dominance of this process in the cooling scenario (over the MU). Asymptotic behaviour of the emissivity $\epsilon[nPBF] \sim 10^{20}T_9^7 \exp(-2\Delta/T)$ for $T \ll \Delta$, $T_9 = T/10^9\text{K}$, as follows from their expression (1b) of [32] and from their rough asymptotic estimate of the integral (see below (13b)), shows up nor a large one nucleon phase space factor ($\sim 10^{28}$) nor appropriate temperature behaviour. Namely this underestimation of the rate in [32] (we again point out that analytic expression (1a) is quite correct) and absence of mentioning of a possible dominance of the process over MU, became a reason that this important result was overlooked during many years. Ref. [24] overlooked sign of anomalous diagram for S pairing and included $\sim g_A^2$ term, where g_A is axial-vector coupling constant, which should be absent in the case of S pairing but being the most important contribution for the $3P_2$ pairing case. In spite of that, a reasonable numerical estimate was presented valid for both S and P pairing including NN correlation effects into consideration. Uncertainty of this numerical value can be estimated by a factor (0.5-1) which is in any case allowed by variation of not too well known correlation factors. Namely this estimate was then incorporated within the cooling code in [26]. Correct asymptotic behaviour of the emissivity is $\epsilon[nPFB, pPFB] \sim 10^{28}(\Delta/\text{MeV})^7(T/\Delta)^{1/2} \exp(-2\Delta/T)$ for $T \ll \Delta$, that showed up a huge one-nucleon phase space factor and very moderate T dependence of the pre-factor. Thereby the value of the rate was related in [24] to the value of the pairing gap. The possibility of the dominant role of this process (even compared to enhanced MMU rather than only MU) was unambiguously stressed. Unfortunately ref. [24] had a number of obvious misprints which were partially corrected in subsequent papers [25,16,35]. Although it does not excuse the authors these misprints can be easily

treated by an *attentive* reader. Ref. [26] was the first that found and quoted the previous result [32].

Ref. [26] incorporated most important in-medium effects in the cooling code, among them nPBF and pPBF as equally important processes. However importance of pPBF process was then overlooked in the subsequent papers where emissivity of this process was several times incorrectly reproduced. Subsequent works [34,35] supported conclusion of [26] on importance of NPBF processes as governing the cooling scenario at $T < T_c$.

The medium modifications of all the above mentioned rates result in a pronounced density dependence (for NPBF processes mainly via dependence of the pairing gaps on the density and the NN correlation factors), which links the cooling behavior of a neutron star decisively to its mass. As the result, the above mentioned medium modifications lead to a more rapid cooling than obtained in the "*standard scenario*". Hence they provide a possible explanation for the observed deviations of some of the pulsar temperatures from the "*standard*" cooling. Particularly, they provide a smooth transition from "*standard*" to "*non-standard*" cooling for increasing central star densities, i.e., star masses. Thus by means of taking into account of most important in-medium effects in the reaction rates one is indeed able to achieve an appropriate agreement with both the high as well as the low observed pulsar temperatures that leads to the new "*nuclear medium cooling scenario*". Using a collection of modern equations of state for nuclear matter in its ground state, which covered both relativistic as well as non-relativistic models, ref. [26] also has demonstrated a relative robustness of the new cooling mechanisms against variations in the equation of state of dense neutron star matter.

At initial stage ($T > T_{opac}$) the newly formed hot neutron star is opaque for neutrinos/antineutrinos. Within FOPE model the value T_{opac} was estimated in [6]. Elastic scatterings were included in ref. [37,38] and pion condensation effect on the opacity was discussed in ref. [39]. Medium effects dramatically affect the neutrino/antineutrino mean free paths, $\lambda_{\nu(\bar{\nu})} \propto 1/|M|^2$, where M is the reaction matrix element. Thereby, one-nucleon elastic scattering processes, like $N\nu \rightarrow N\nu$, are suppressed by NN correlations [24,16,40,41]. However neutrino/antineutrino absorption in two-nucleon MMU and MNB processes increases with the density (since $|M|^2$ of MMU and MNB processes increase with the density) [23,24,16]. Thus more massive neutron stars are opaque for neutrinos/antineutrinos up to lower temperatures that also results in a delay of neutrino/antineutrino puls. Within the quasiparticle approximation for the nucleons the value T_{opac} was estimated with taking into account medium effects in refs [23,16]. Refs [42,43,16] considered possible consequences of such a delay for supernova explosions. On the other hand at $T > (1 - 2)\text{MeV}$ one should take care of the neutrino/antineutrino radiation in multiple NN scatterings (Landau–Pomeranchuk–Migdal effect) when averaged neutrino–antineutrino energy, $\omega_{\nu\bar{\nu}} \sim \text{several } T$, becomes to be smaller than the nucleon width Γ_N [28]. Numerical evaluations of Γ_N in application to MNB processes were done in [76] and [77] within the Bruckner scheme and using Bethe–Salpeter

equation for nucleons. The Landau–Pomeranchuk–Migdal effect suppresses the rates of the neutrino elastic scattering processes on nucleons and also it suppresses MNB rates. For neutron stars of rather low mass ($\lesssim M_\odot$) the suppression of the rates of neutral current processes due to NN correlations and the multiple collision coherence effect prevail the enhancement due to the pion softening, and for sufficiently massive neutron stars ($\gtrsim 1.4M_\odot$) the enhancement prevails the suppression. MMU emissivity remains to be almost unaffected by the Landau–Pomeranchuk–Migdal effect since averaged $\bar{\nu}e$ energy $\sim p_{Fe}$ is rather large $\gg \Gamma_N$.

The paper is organized as follows. Sect. 2 discusses basic ideas of the Landau–Migdal Fermi liquid approach. The NN interaction amplitude is constructed with an explicit treatment of long-ranged soft pion degree of freedom and vertex renormalizations due to NN correlations. The meaning of the pion softening effect is clarified and a comparison for NN cross sections evaluated in MOPE and FOPE models is given. Then the renormalization of weak interaction in neutron star matter is performed. Sect. 3 discusses cooling of non-superfluid neutron stars ($T_{opac} > T > T_c$). We start with a demonstration that it is theoretically inconsistent to describe NN interaction with the help of vacuum cross section at the same time considering pions as freely propagating particles in matter. This inconsistency will lead us to a problem which will be then resolved within a consistent Fermi liquid approach. The comparison of emissivities of MMU and MU processes shows a significant enhancement of in-medium rates. Then we discuss DU-like processes and demonstrate a suppression effect due to vertex renormalizations. Demonstration of the role of in-medium mechanisms in the calculation of the cooling evolution of neutron stars within a realistic cooling code is given in next Section. Then we consider influence of in-medium effects on the neutrino mean free path at initial stage of neutron star cooling. Essential role of multiple NN collisions (Landau–Pomeranchuk–Migdal effect) is shown. Sect. 4 presents OTF in non-equilibrium closed diagram technique in the framework of quasiparticle approximation for the nucleons and then beyond the quasiparticle approximation incorporating particle width effects.

2 Fermi Liquid Behaviour of Baryon Matter

2.1 A general strategy - separation of soft and hard modes

We will restrict ourselves by consideration of the nuclear matter at densities less than about $5\rho_0$, where $\rho_0 \simeq 0.17 \text{ fm}^{-3}$ is the normal nuclear matter density, and at typical excitation energies (temperatures) which are very low compared to those essentially involving quark-gluon degrees of freedom ($\sim 1/r_\Lambda$, where $r_\Lambda \sim (0.2 - 0.3) \text{ fm}$ is the confinement radius). Then, we may deal with baryon-meson degrees of freedom rather than with the quark-gluon ones. Thus, we suppose that baryons interact via meson (pion, sigma, rho, omega, etc.) exchanges.

Different processes involved in nuclear phenomena occurring on hadron level are characterized by the corresponding space-time and energy-momentum scales. Of the order of the confinement radius r_Λ are scales associated with heavy mesons such as σ and Ω mesons ($r \sim r_\sigma \sim 1/m_\sigma$, $r \sim r_\Omega \sim 1/m_\Omega$) and with nucleons, $r_N \sim 1/m_N$. We will treat these scales as short-ranged. Typical low momenta in our consideration will be $k \sim m_\pi$ and $k \sim p_F \sim 1/(2m_\pi)$, where p_F is Fermi momentum of nucleon, that corresponds to the length scales $r \sim 1/m_\pi$ and $r \sim 1/p_F$, respectively. These latter scales will be treated as rather long-ranged microscopic scales. Time scales, which correspond to low energies are $\sim 1/\epsilon_F$ (ϵ_F is the Fermi energy of nucleons, $\sim 1/m_\pi$ and $\sim 1/\omega_\Delta$ ($\omega_\Delta = m_\Delta - m_N \simeq 2.1m_\pi$ is the energy gap for the excitation of Δ isobars)). Δ isobars should therefore be treated as long-ranged excitations in our scales. Besides they have a large spin-isospin degeneracy factor (16) compared to that for nucleons (4) and more strongly coupled to the pions ($f_{\pi N\Delta} \simeq 2.151/m_\pi$ whereas $f_{\pi N} \simeq 1/m_\pi$). Especial role here belongs to the pion mode. The saturation nuclear density is $\rho_0 \simeq 0.48m_\pi^3$, i.e. of order of unit in these natural interaction units. Already from this simple observation one can conclude first that pion takes essential part in gluing of nuclear matter and second, that the nucleon–nucleon interaction and, in particular, long-range part of this interaction at $\rho \gtrsim \rho_0$ should essentially differ from those in vacuum. Thereby, there is, actually, no hope that perturbative schemes could help in construction of a proper description of nucleon matter for $\rho \gtrsim \rho_0$. In such a situation, one should expect strong in-medium effects, especially for pions, being the lightest among hadrons ($m_\pi/m_N \simeq 1/7$). Minimal energy scale related to this long-range part of NN interaction is *the effective pion gap* $\tilde{\omega} \leq m_\pi$. The value $\tilde{\omega}^2$ replaces the corresponding value $\simeq m_\pi^2 + p_F^2$ characterizing FOPE contribution to NN interaction, cf. [16]. The energy scale $\tilde{\omega}$ arises due to a peculiar collective *pion softening effect* appearing for nucleon densities $\rho > \rho_{c1} \simeq (0.5-0.7)\rho_0$ due to a strong P wave πN attraction discovered by Migdal [44,67,16]. Presence of this soft mode becomes of prime importance. As ions in solids interact mainly by phonons, i.e. by soft collective modes being absent in vacuum, as nucleons in a dense nucleon matter interact via the collective modes the dominant among which is the softest one. The latter is the particle-hole mode with the pion quantum numbers.

2.2 Description of NN interaction

At temperatures of our interest ($\ll \epsilon_{Fn}$) neutrons are only slightly excited above their Fermi sea and all the processes occur in a narrow vicinity of ϵ_{Fn} . In such a situation Fermi liquid approach seems to be the most efficient one. Within this approach the long-ranged diagrams are treated explicitly whereas short-scale diagrams are treated as local quantities given by phenomenological so called Landau-Migdal parameters. Thus using argumentation of Fermi liquid theory [46,47,67,16] the retarded NN interaction amplitude is presented as follows

The diagram shows an equation for a four-point interaction. On the left is a contact diagram with four external lines meeting at a central square vertex. This is equal to the sum of three diagrams: 1) a contact diagram with a shaded central square vertex, 2) an exchange diagram with two shaded circular vertices connected by two horizontal lines, and 3) an exchange diagram with two shaded circular vertices connected by two horizontal lines, with an additional internal loop structure. The equation is labeled (1) on the right.

where



$$(2)$$

The solid line presents the nucleon, whereas double-line, the Δ isobar. The empty-dotted line corresponds to the exchange of the free pion with inclusion of the contributions of the residual S wave πNN interaction and $\pi\pi$ scattering, i.e. the irreducible residual interaction to the nucleon particle-holes and delta-nucleon holes. The full particle-hole, delta-nucleon hole and pion irreducible block in eq. (1) is by its construction essentially more local then contributions given by explicitly presented graphs. Thereby, it is parameterized with the help of the so called Landau–Migdal parameters. In the standard Landau Fermi liquid theory fermions are supposed to be at their Fermi surface and the Landau parameters are expanded in Legendre polynomials in the angle between fermionic momenta. Luckily, only zero and first harmonics enter physical quantities. The momentum dependence of nuclear forces is not as pronounced and one has no need to do this expansion. Then these parameters, i.e. f_{nn} , f_{np} and g_{nn} , g_{np} in scalar and spin channels respectively, can be considered as slightly momentum dependent quantities. They can be evaluated as functions of density, neutron and proton concentrations, energy and momentum.

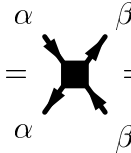
The part of interaction involving Δ is analogously constructed



$$(3)$$

The main part of the $N\Delta$ interaction is due to the pion exchange. Although information on local part of the $N\Delta$ interaction is rather scarce one can conclude [16,19] that the corresponding Landau–Migdal parameters are essentially smaller then those for NN interaction. Besides, at small transferred energies $\omega \ll m_\pi$ the Δ –nucleon hole contribution is a smooth function of ω and k in difference with the nucleon–nucleon hole contribution. Therefore and for the sake of simplicity we neglect the first graph in r.h.s. of eq. (3).

Straightforward resummation of (1) in neutral channel yields



$$\Gamma_{\alpha\beta}^R = C_0 \left(\mathcal{F}_{\alpha\beta}^R + \mathcal{Z}_{\alpha\beta}^R \vec{\sigma}_1 \cdot \vec{\sigma}_2 \right) + f_{\pi N}^2 \mathcal{T}_{\alpha\beta}^R (\vec{\sigma}_1 \cdot \vec{k}) (\vec{\sigma}_2 \cdot \vec{k}), \quad (4)$$

$$\begin{aligned} \mathcal{F}_{\alpha\beta}^R &= f_{\alpha\beta} \gamma(f_{\alpha\beta}), \quad \mathcal{Z}_{nn}^R = g_{nn} \gamma(g_{nn}), \quad \mathcal{Z}_{np}^R = g_{np} \gamma(g_{nn}), \quad \alpha, \beta = (n, p), \\ \mathcal{T}_{nn}^R &= \gamma^2(g_{nn}) D_{\pi^0}^R, \quad \mathcal{T}_{np}^R = -\gamma_{pp} \gamma(g_{nn}) D_{\pi^0}^R, \quad \mathcal{T}_{pp}^R = \gamma_{pp}^2 D_{\pi^0}^R, \\ \gamma^{-1}(x) &= 1 - 2C_0 x A_{nn}^R, \quad \gamma_{pp} = (1 - 4C_0 g A_{nn}^R) \gamma(g_{nn}), \end{aligned} \quad (5)$$

$f_{nn} = f_{pp} = f + f'$, $f_{np} = f - f'$, $g_{nn} = g_{pp} = g + g'$, and $g_{np} = g - g'$, C_0 is dimensional normalization factor which is usually taken to be $C_0 = \pi^2/[m_N p_F(\rho_0)] \simeq 300$ MeV.

$\text{fm}^3 \simeq 0.77m_\pi^{-2}$, $D_{\pi^0}^R$ is the full retarded Green function of π^0 , $A_{\alpha\beta}$ is the corresponding (nn) nucleon–nucleon hole loop

$$A_{\alpha\beta} = \begin{array}{c} \beta \\ \circlearrowleft \\ \alpha^{-1} \end{array} \quad (6)$$

and we for simplicity neglect proton hole contributions due to a small concentration of protons in the neutron star matter.

Resummation of (1) in the charged channel yields

$$\tilde{\Gamma}_{np}^R = \begin{array}{c} n \quad n \\ \diagup \quad \diagdown \\ \blacksquare \\ \diagdown \quad \diagup \\ p \quad p \end{array} = C_0 \left(\tilde{\mathcal{F}}_{np}^R + \tilde{\mathcal{Z}}_{np}^R \vec{\sigma}_1 \cdot \vec{\sigma}_2 \right) + f_{\pi N}^2 \tilde{\mathcal{T}}_{np}^R (\vec{\sigma}_1 \cdot \vec{k})(\vec{\sigma}_2 \cdot \vec{k}), \quad (7)$$

$$\tilde{\mathcal{F}}_{np}^R = 2f'\tilde{\gamma}(f'), \quad \tilde{\mathcal{Z}}_{np}^R = 2g'\tilde{\gamma}(g'), \quad \tilde{\mathcal{T}}_{np}^R = \tilde{\gamma}^2(g')D_{\pi^-}^R, \quad \tilde{\gamma}^{-1}(x) = 1 - 4C_0 x A_{np}^R. \quad (8)$$

The Landau–Migdal parameters are rather unknown for isotopically asymmetric nuclear matter and for $\rho > \rho_0$. Although some evaluations of these quantities have been done, much work is still needed to get convincing results. Therefore for estimates we will use the values extracted from atomic nucleus experiments. Using argumentation of a relative locality of these quantities we will suppose the Landau–Migdal parameters to be independent on the density for $\rho > \rho_0$. One then can expect that the most uncertain will be the value of the scalar constant f due to essential role of the medium-heavy σ meson in this channel. But this parameter does not enter the tensor force channel being most important in our case. Unfortunately, there are also essential uncertainties in numerical values of some of the Landau–Migdal parameters even for atomic nuclei. These uncertainties are, mainly, due to attempts to get the best fit to experimental data in each concrete case slightly modifying parameterization used for the residual part of the NN interaction. E.g., calculations [47] gave $f \simeq 0.25$, $f' \simeq 1$, $g \simeq 0.5$, $g' \simeq 1$ whereas refs [48–50], including quasiparticle renormalization pre-factors, derived the values $f \simeq 0$, $f' \simeq 0.5 - 0.6$, $g \simeq 0.05 \pm 0.1$, $g' \simeq 1.1 \pm 0.1$.

Typical energies and momenta entering NN interaction of our interest are $\omega \simeq 0$ and $k \simeq p_{Fn}$. Then rough estimation yields $\gamma^{-1}(g', \omega \simeq 0, k \simeq p_{Fn}, \rho = \rho_0) \simeq 0.3 - 0.45$. For $\omega = k \simeq T$ typical for the weak processes with participation of $\nu\bar{\nu}$ one has $\gamma^{-1}(g', \omega \simeq k \simeq T, \rho = \rho_0) \simeq 0.7 - 0.9$.

2.3 Virtual Pion Mode of NN Interaction.

Resummation of the diagrams yields the following Dyson equation for pions

$$\text{wavy line} = \text{wavy line} + \text{wavy line} \circlearrowleft \text{triangle} + \text{wavy line} \circlearrowleft \text{triangle with dot} + \text{wavy line} \boxed{\Pi_{\text{reg}}^R} \text{wavy line} \quad (9)$$

The $\pi N\Delta$ full-dot-vertex includes a background correction due to the presence of the higher resonances, Π_{res}^{ret} is the residual retarded pion self-energy that includes the contribution of all the diagrams which are not presented explicitly in eq. (9). The full vertex takes into account NN correlations

$$\text{Diagram 1} = \text{Diagram 2} + \text{Diagram 3} \quad (10)$$

Due to that the nucleon particle-hole part of Π_{π^0} is $\propto \gamma(g_{nn})$ and the nucleon particle-hole part of Π_{π^\pm} is $\propto \gamma(g')$. The value of the NN interaction in the pion channel is determined by the full pion propagator at small ω and $k \simeq p_{Fn}$, i.e. by the quantity $\tilde{\omega}^2(k) = -(D_\pi^R)^{-1}(\omega = 0, k, \mu_\pi)$. Typical momenta of our interest are $k \simeq p_{Fn}$. Indeed the momenta entering the NN interaction in MU and MMU processes are $k = p_{Fn}$, the momenta governing the MNB are $k = k_0$ [23] where the value $k = k_0 \simeq (0.9 - 1)p_{Fn}$ corresponds to the minimum of $\tilde{\omega}^2(k)$. The quantity $\tilde{\omega} \equiv \tilde{\omega}(k_0)$ has the meaning of the *effective pion gap*. It is different for π^0 and for π^\pm since neutral and charged channels are characterized by different diagrams permitted by charge conservation, thus also depending on the value of the pion chemical potential, $\mu_\pi^+ \neq \mu_\pi^- \neq 0$, $\mu_\pi^0 = 0$. For $T \ll \epsilon_{Fn}, \epsilon_{Fp}$ these chemical potentials are $\mu_\pi^- = \mu_e = \epsilon_{Fn} - \epsilon_{Fp}$, $\mu_\pi^+ = \epsilon_{Fn}$, as follows from equilibrium conditions for the reactions $n \rightarrow p\pi^-$, $p \rightarrow n\pi^+$ and $n \rightarrow pe\bar{\nu}$.

Change the sign of $\tilde{\omega}^2$ symbolizes the pion condensate phase transition. Typical density behaviour of $\tilde{\omega}^2$ is shown in Fig. 3. At low densities ($\rho < (0.5 - 0.7)\rho_0$),

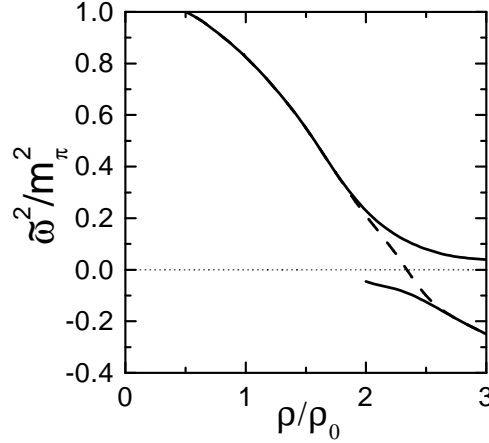


Fig. 3. Effective pion gap (for $\mu_{\pi^0} = 0$) versus baryon density, see ref. [16].

$\text{Re}\Pi_\pi^R$ is small and one has $\tilde{\omega}^2 = m_\pi^2 - \mu_\pi^2$. For such densities the value $\tilde{\omega}^2(p_{Fn})$ essentially deviates from $m_\pi^2 - \mu_\pi^2$ tending to the value $m_\pi^2 + p_{Fn}^2 - \mu_\pi^2$ only in small density limit. Approximately one has $\mu_{\pi^-} = p_{Fe} = p_{Fp} = p_{Fn}/2$.

The dashed line describes the case where $\pi\pi$ fluctuations are artificially switched off and the phase transition turns out to be of the second order. At the critical point of the pion condensation ($\rho = \rho_{c\pi}$) this value of $\tilde{\omega}^2$ with switched off $\pi\pi$ fluctuations changes its sign. In reality the $\pi\pi$ fluctuations are significant in the vicinity of the

critical point and there occurs the first-order phase transition to the inhomogeneous pion-condensate state [51,59,53]. Thereby there are two branches (solid curves in Fig. 3) with positive and respectively negative value for $\tilde{\omega}^2$. Calculations of ref. [53] demonstrated that at $\rho > \rho_{c\pi}$ the free energy of the state with $\tilde{\omega}^2 > 0$, where the pion mean field is zero, becomes larger than that of the corresponding state with $\tilde{\omega}^2 < 0$ and a finite mean field. Therefore at $\rho > \rho_c$ the state with $\tilde{\omega}^2 > 0$ is metastable and the state with $\tilde{\omega}^2 < 0$ and the pion mean field $\varphi_\pi \neq 0$ becomes the ground state.

The quantity $\tilde{\omega}^2$ demonstrates how much the virtual (particle-hole) mode with pion quantum numbers is softened at given density. The ratio $\alpha = D_\pi[\text{med.}]/D_\pi[\text{vac.}] \simeq 6$ for $\rho = \rho_0$ and for isospin symmetric nuclear matter. However this essential so called "*pion softening*" does not significantly enhance the NN scattering cross section due to a simultaneous suppression of πNN vertex by NN correlations. Estimation of the rate of the NN cross sections calculated via FOPE and MOPE yields

$$R = \frac{\sigma[\text{FOPE}]}{\sigma[\text{MOPE}]} \simeq \frac{\gamma^4(g', \omega \simeq 0, k \simeq p_{FN})(m_\pi^2 + p_{FN}^2)}{\tilde{\omega}^4}. \quad (11)$$

For $\rho = \rho_0$ one has $\gamma(g', \omega \simeq 0, k \simeq p_{FN}) \simeq 0.3 - 0.4$, $\tilde{\omega}^2 \simeq 0.8$, $p_{FN} \simeq 2m_\pi$ and $R \lesssim 1$, whereas for $\rho = 2\rho_0$ with our rough estimates one already gets $R \sim 10$.

As follows from numerical estimates of different γ factors entering (4) and (7) the most important contribution to NN interaction for $\rho > \rho_0$ is given by MOPE

$$\text{[Diagram: A thick black vertical bar representing a tensor force]} \simeq \text{[Diagram: A wavy line with arrows at both ends representing a pion exchange]} \quad (12)$$

whether this channel ($\mathcal{T} \propto (\vec{\sigma}_1 \cdot \vec{k})(\vec{\sigma}_2 \cdot \vec{k})$) of the reaction is not forbidden or suppressed by some specific reasons like symmetry, small momentum transfer, etc. Thus instead of FOPE, as the model of NN interaction which has been used in [6] in calculation of the emissivities of two-nucleon reactions within the "*standard scenario*" of neutron star cooling one needs to use the full NN interaction given by eqs (4) and (7) or, simplifying, approximated by its MOPE part.

Some doubts were expressed in connection to the role of the ρ meson part of tensor forces. Ref. [6] estimated ρ meson contribution to MU emissivity arguing for a suppression of FOPE contribution by factor of 2. Let us estimate how much is essential a contribution of the ρ meson to the tensor forces. Using identity $(\vec{\sigma}_1 \times \vec{k})(\vec{\sigma}_2 \times \vec{k}) = k^2 \vec{\sigma}_1 \vec{\sigma}_2 - (\vec{\sigma}_1 \vec{k})(\vec{\sigma}_2 \vec{k})$ the ρ exchange interaction can be cast in the form

$$\delta\Gamma_{N_1 N_2}^R = \left(\frac{f_\rho}{m_\rho}\right)^2 \left\{ \frac{k^2(\vec{\sigma}_1 \vec{\sigma}_2)\gamma^2}{[\omega^2 - m_\rho^2 - k^2 - \Pi_\rho^R]} - \frac{(\vec{\sigma}_1 \vec{k})(\vec{\sigma}_2 \vec{k})\gamma^2}{[\omega^2 - m_\rho^2 - k^2 - \Pi_\rho^R]} \right\}. \quad (13)$$

We may omit contribution $\text{Re}\Pi_\rho^R$ in the Green function since $\text{Re}\Pi_\rho^R \ll m_\rho^2$ for $\rho \sim m_\pi^3$ under consideration; γ factor is the same as for the corresponding pion (charged or neutral). First term is supposed to be included in phenomenological value of the corresponding Landau–Migdal parameter leading to its momentum dependence. Due to that the value g' gets a 30% decrease (rather than an increase discussed in some works) with the momentum at $k = p_{FN}$ compared to the corresponding value at $k = 0$, see [56]. Thus one can think that $g'(0) > g'(p_{FN})$. Second term can be dropped as small ($\lesssim 1/30$ of MOPE contribution at $\rho = \rho_0$).

Another worry [57,58] was expressed in connection with experimental quasielastic polarization transfer experiment at LAMPF, EMC experiment and the Drell–Yan experiment at Fermi Lab which did not observe an expected in several works a pronounced pion excess in nuclei. First optimistic estimates demonstrated the pion excess to be at (15-30)% level that was ruled out by different model analysis of mentioned experimental results which included artificially enhanced pion contribution and suppressed other important contributions. There were also many rather naive speculations which expected the excess to essentially grow in the vicinity of the pion condensation point for $(T = 0)$.²

First let us to briefly discuss the physical origin of the effect. Let us estimate a contribution of the virtual pion sea (region of small energies $\omega < kv_F$) to the full sum rule. It is given by

$$S(kv_F) = \int_0^{kv_F} 2\omega A_\pi \frac{d\omega}{2\pi} = \frac{2}{\pi\beta} \left[kv_F - \frac{\tilde{\omega}^2(k)}{\beta} \arctan \left(\frac{\beta kv_F}{\tilde{\omega}^2(k)} \right) \right] \ll 1,$$

$$S(\infty) = 1, \quad \beta = \frac{m_N^{*2} k f_{\pi N}^2}{\pi^2}, \quad (14)$$

m_N^* is the nonrelativistic effective mass given by the relation $(d\epsilon(p)/dp)|_{p_F} = p_F/m^*$. The quantity $S(kv_F)$ having no singularity even at $\tilde{\omega}^2(k_0) \rightarrow 0$ is, thus, rather insensitive to the pion softening effect. Therefore it seems clear that the mentioned experimental analysis is not critical to the value $\tilde{\omega}^2(k_0)$. This point was missed in previous analysis of the pion excess. The physical reason of a non-zero contribution of virtual pions to the sum-rule at $\omega < kv_F$ is clear. It is just the well known Landau damping associated with the possibility of the virtual pion decay to the nucleon particle and the hole, i.e. just with the Pauli blocking. As known from πN scattering experiments, pions interact with nucleons. Thus must be a contribution to the sum-rule. There is no other way out. Therefore on a question "Where virtual pions are?" we would still suggest an old fashion answer: "They are hidden inside the matter". The question which remains is only "What is the actual value of the pion excess?" To properly answer it one needs besides the pionic contribution to elaborate all relevant specific contributions related to the phenomenon analysed in the given concrete experiment. E.g., quasielastic polarization transfer data are

² For $T \neq 0$ this excess indeed essentially grows in the vicinity of the critical point [?].

reasonably fitted with a slightly increased value of the Landau–Migdal parameter g' and with inclusion of S wave repulsion at small energies [16,60,61], EMC experiment is reproduced with inclusion of the soft pion mode and other relevant effects [62], Drell-Yan production is described with taking into account of nucleon binding [63] and initial state interactions of fast partons [64] with the pion excess included (although in [64] the later is taken in a rather naive model where the pion excess is artificially increased).

2.4 Renormalization of the Weak Interaction.

The full weak coupling vertex that takes into account NN correlations is determined by eq. (15) where now the wavy line should be replaced by the lepton pair.

Thus for the vertex of our interest, $N_1 \rightarrow N_2 l \bar{\nu}$, we obtain

$$V_\beta = \frac{G}{\sqrt{2}} [\tilde{\gamma}(f')l_0 - g_A \tilde{\gamma}(g')\vec{l}\vec{\sigma}], \quad (16)$$

for the β decay and

$$V_{nn} = \frac{G}{2\sqrt{2}} [\gamma(f_{nn})l_0 - g_A \gamma(g_{nn})\vec{l}\vec{\sigma}], \quad V_{pp} = \frac{G}{2\sqrt{2}} [\kappa_{pp}l_0 - g_A \gamma_{pp}\vec{l}\vec{\sigma}], \quad (17)$$

$$\kappa_{pp} = c_V - 2f_{np}C_0 A_{nn}\gamma(f_{nn}), \quad \gamma_{pp} = (1 - 4gC_0 A_{nn})\gamma(g_{nn}), \quad (18)$$

for the processes on the neutral currents $N_1 N_2 \rightarrow N_1 N_2 \nu \bar{\nu}$. Here $G \simeq 1.17 \cdot 10^{-5} \text{ GeV}^{-2}$ is the Fermi weak interaction constant, $c_V = 1 - 4 \sin^2 \theta_W$, $\sin^2 \theta_W \simeq 0.23$, $g_A \simeq 1.26$ is the axial-vector interaction coupling constant, and $l_\mu = \bar{u}(q_1)\gamma_\mu(1 - \gamma_5)u(q_2)$ is the lepton current. The tensor force contribution $\sim \vec{q}^2$ is small for typical $|\vec{q}| \simeq T$ or p_{Fe} , and for the sake of simplicity is omitted.

The γ factors renormalize the corresponding vacuum vertices. These factors are essentially different for different processes involved. The matrix elements of the neutrino/antineutrino scattering processes $N\nu \rightarrow N\nu$ and of MNB, $NN \rightarrow NN\nu\bar{\nu}$, behave differently in dependence whether $N = n$ or $N = p$ in the weak coupling vertex. Vertices

are modified by the correlation factors (5) and (8). For $N = n$ these are $\gamma(g_{nn}, \omega = q \simeq T)$ and $\gamma(f_{nn}, \omega = q \simeq T)$ which are $\simeq 0.7 - 0.9$ leading to the suppression of the corresponding cross sections by $0.5 - 0.8$. Renormalization of the proton vertex is determined by the processes

$$(20)$$

being forbidden in vacuum. For the systems with $1S_0$ proton-proton pairing, $\propto g_A^2$ contribution to the squared matrix element from the first diagram is compensated by the corresponding contribution of the diagram with anomalous Green functions of protons. The vector current term is $\propto c_V^2$ in vacuum. Thereby the corresponding vertices with participation of proton ($N = p$) in medium are enhanced compared to the small vacuum value ($\propto c_V^2 \simeq 0.06$) leading to the enhancement of the cross sections by $\sim 10^2$ times. Also contribution of the same order of magnitude may come from the intermediate in-medium photon γ_m whose propagator contains $1/\omega_{pl}^2 \sim 1/e^2$ (or $1/m_\gamma^2 \sim 1/e^2$ in superconducting proton medium) that compensates small e^2 factor from electromagnetic vertices [54]. Other permitted intermediate states like processes with pp^{-1} and with the pion are suppressed, the former by a small proton density factor and the latter by small $q^2 \sim T^2$ pre-factors. First diagram was considered already in [24] where the pPBF process was suggested, and then in [26], and it was shown that nPBF and pPBF processes may give contributions of the same order of magnitude. Several subsequent papers overlooked these results and rediscovered the pPBF process considering its rate as small since they ignored the nucleon and the electron correlation effects. Specific contribution of second diagram was recently discussed in [55] in association with pPBF process. First diagram was overlooked. The sub-process

$$(21)$$

of $\bar{\nu}$ scattering on nucleus with excitation of in-medium K^- is dramatically modified by in-medium effects [27]. The μ^+ production cross section is larger than the positron one by a factor ≈ 4 in contrast to expectation based upon the vacuum branching ratios of a kaon decay $\Gamma(K^- \rightarrow e^- + \nu_e)/\Gamma(K^- \rightarrow \mu^- + \nu_\mu) \approx 2.5 \times 10^{-5}$. For the bare weak interaction the squared matrix element of the reaction $\bar{\nu}_l \rightarrow K^- + l^+$ would be $|\mathcal{M}|^2 \propto m_l^2[m_l^2 - (k \cdot k)]/2$, that explains a strong enhancement of muon processes in vacuum compared to the positron ones. In medium the weak kaon current is dramatically modified due to the mixture of kaons with the

Λ -particle-proton hole states carrying the same quantum numbers

$$\text{Diagram 1} = \text{Diagram 2} + \text{Diagram 3} \quad (22)$$

As the result, the squared matrix element of the reaction does not possess strong dependence on the lepton mass. Therefore, in medium squared matrix elements for positrons and muons turn out to be of the same order of magnitude.

Thus we see that in dependence of what reaction channel is considered in-medium effects may or strongly enhance the reaction rate under consideration or substantially suppress it.

2.5 Inconsistency of FOPE Model for the Description of NN Interaction in Dense Matter

Since FOPE model became the base of the "standard scenario" for cooling simulations we would like first to demonstrate principal inconsistencies of the model for the description of interactions in dense ($\rho \gtrsim \rho_0$) baryon medium. The only diagram existing in FOPE model which contributes to the neutrino emissivity of two-nucleon processes is as follows

$$\text{Diagram (23)} \quad (23)$$

Dots symbolize FOPE. This is first available Born approximation diagram, i.e. second order perturbative contribution in $f_{\pi N}^2$. Then in order to be theoretically consistent one should use perturbation theory up to the very same second order in $f_{\pi N}$ for all the quantities. E.g., pion spectrum is determined by pion polarization operator expanded up to the very same second order in $f_{\pi N}^2$

$$\omega^2 = m_\pi^2 + k^2 + \Pi^0(\omega, k, \rho), \quad \Pi^0(\omega, k, \rho) = \text{Diagram (24)} \quad (24)$$

The value $\Pi^0(\omega, k, \rho)$ is easily calculated containing no any uncertain parameters. For the values $\omega \rightarrow 0$ and $k \simeq p_F$ of our interest one gets

$$\Pi^0 \simeq -\alpha_0 + i\beta_0\omega, \quad \alpha_0 = \frac{2m_N p_F k^2 f_{\pi N}^2}{\pi^2} > 0, \quad \beta_0 = \frac{m_N^2 k f_{\pi N}^2}{\pi} > 0. \quad (25)$$

Replacing this value to eq. (24) we obtain a solution with $i\omega < 0$ already for $\rho > 0.2\rho_0$ that would mean appearance of the pion condensation. Indeed, the mean field

$$+ \dots \quad (27)$$

whereas the third diagram which naturally generalizes the corresponding MU(FOPE) contribution gives only a small correction for $\rho \gtrsim \rho_0$, [23,42,43,16]. The resulting emissivity given by two first diagrams in a simplified notation reads as follows, see ([16,26]),

$$\epsilon^{MMU}[\text{MOPE}] \simeq 2.4 \times 10^{24} T_9^8 \left(\frac{\rho}{\rho_0} \right)^{10/3} \frac{(m_n^*)^3 m_p^*}{m_N^4} \left[\frac{m_\pi}{\alpha \tilde{\omega}_{\pi^0}(p_{Fn})} \right]^4 \left[\frac{m_\pi}{\alpha \tilde{\omega}_{\pi^\pm}(p_{Fn})} \right]^4 \times \Gamma^8 F_1 \zeta(\Delta_n) \zeta(\Delta_p) \frac{\text{erg}}{\text{cm}^3 \text{sec}}, \quad (28)$$

where $T_9 = T/10^9$ K is the temperature, m_n^* and m_p^* are the nonrelativistic effective neutron and proton masses, respectively,

$$\Gamma^8 = \gamma_\beta^2(\omega \simeq p_{Fe}, q \simeq p_{Fe}) \gamma^2(g_{nn}, \omega \simeq 0, k = p_{Fn}) \tilde{\gamma}^4(g', 0, p_{Fn}),$$

$$\gamma_\beta^2(\omega, q) = \frac{\tilde{\gamma}^2(f', \omega, q) + 3g_A^2 \tilde{\gamma}^2(g', \omega, q)}{1 + 3g_A^2}, \quad (29)$$

and the second term in the factor

$$F_1 = 1 + \frac{3}{4\tilde{\gamma}^2(g', 0, p_{Fn})} \left(\frac{\rho}{\rho_0} \right)^{2/3} \quad (30)$$

is the contribution of the pion decay from intermediate states (first diagram). The quantity Γ effectively accounts for a product of the NN correlation factors in different $\pi N_1 N_2$ vertices. For charged pions the value $\mu_\pi \neq 0$ is incorporated in the expression for the effective pion gap, for neutral pions $\mu_\pi = 0$. The value of the parameter α is given by $\alpha = 1$ for $\rho < \rho_{c\pi}$, and $\alpha = \sqrt{2}$ for $\rho > \rho_{c\pi}$ taking account of the new excitations on the ground of the π condensate vacuum. The factor

$$\zeta(\Delta_N) \simeq \begin{cases} \exp(-\Delta_N/T) & T \leq T_{cN}, \\ 1 & T > T_{cN}, \quad N = (n, p), \end{cases} \quad (31)$$

estimates the suppression caused by the neutron–neutron and proton–proton pairings. A deviation of these factors from simple exponents can be incorporated as in ref. [33].

The ratio of the emissivities of MMU(MOPE) and MU(FOPE) is roughly as follows

$$\frac{\epsilon^{MMU}[\text{MOPE}]}{\epsilon^{MU}[\text{FOPE}]} \simeq 10^3 \frac{\gamma^2(g_{nn}, 0, p_{Fn}) \tilde{\gamma}^2(g', 0, p_{Fn}) \tilde{\gamma}^2(g', p_{Fe}, p_{Fe})}{\tilde{\omega}_{\pi^0}^4(p_{Fn}) \tilde{\omega}_{\pi^\pm}^4(p_{Fn})} (\rho/\rho_0)^{10/3}. \quad (32)$$

For $\rho \simeq \rho_0$ this ratio is ~ 10 whereas being estimated with the only third diagram (27) it would be less than unit.

3.2 Emissivity of DU-like processes

NPBF processes. The one-nucleon processes with neutral currents given by the second diagram (19) for $N = n$ and p are forbidden at $T > T_c$ by energy-momentum conservation law but they can occur at $T < T_c$. Then physically the processes relate to NPBF, see Fig.2. However they need a special technique to be calculated, see [32,24].

These processes $n \rightarrow n\nu\bar{\nu}$ and $p \rightarrow p\nu\bar{\nu}$ play very important part in the cooling of superfluid neutron stars, see [24,25,16,26,34,33]. The emissivity for 3 types of neutrinos is given by [24,25]³

$$\begin{aligned} \epsilon[\text{nPBF}]_n &= \frac{3 \cdot 4G^2 (\xi_1 \gamma^2(f_{nn}) + \xi_2 g_A^2 \gamma^2(g_{nn})) p_{Fn} m_n^* \Delta_n^7}{15\pi^5} I(\Delta_n/T) \\ &\simeq \zeta \times 10^{28} (\rho/\rho_0)^{1/3} (m_n^*/m_N) (\Delta_n/\text{MeV})^7 I(\Delta_n/T), \quad \frac{\text{erg}}{\text{cm}^3 \cdot \text{sec}}, \quad T < T_{cn}, \quad (33) \end{aligned}$$

where $G \simeq 1.17 \cdot 10^{-7} \text{GeV}^{-2}$ is Fermi constant of weak interaction, Δ_n is the neutron gap, T_{cn} is critical temperature for neutron pairing, $\xi_1 = 1$, $\xi_2 = 0$ for S -pairing and $\xi_1 = 2/3$, $\xi_2 = 4/3$ for P -pairing, cf. [33]. For typical neutrino energies $\omega_q = q$ correlations are not so essential as it is for $\omega \ll q$. Taking $\gamma^2 \simeq 0.9$ in the range of S -pairing we get $\zeta \simeq 3$ whereas with $\gamma^2 \simeq 0.7$ for a more dense region of P -pairing we obtain $\zeta \simeq 6.6$, in agreement with numerical evaluations [24] used within the cooling code in ref. [26], $I(x) = \int_0^\infty \text{ch}^5 y dy / (\exp(x \text{ch} y) + 1)^2$. One should notice that this numerical estimate is by a factor of $(20 \div 50)$ larger than that in [32]. The emissivity of the process $p \rightarrow p\nu\bar{\nu}$ is given by [24]

$$\epsilon(p \rightarrow p\nu\bar{\nu}) = \frac{3 \times 4G^2 (\xi_1 \kappa_{pp}^2 + \xi_2 g_A^2 \gamma_{pp}^2 + \xi_3) p_{Fp} m_p^* \Delta_p^7}{15\pi^5} I(\Delta_p/T), \quad T < T_{cp}, \quad (34)$$

Δ_p is the proton gap, T_{cp} is critical temperature for pairing of protons, which are paired in S -state in neutron star matter, The vertex corrections take into account nucleon–nucleon correlations, $\xi_3 \lesssim 1$ is due to the second diagram (20) and has a

³ Here I remove some misprints existed in [32,24,25,16].

complicated structure [54,55]. In the process (34) a part of NN correlations is especially important. One has $\kappa_{pp}^2 \simeq 1$ instead of a small $c_V^2 \simeq 0.006$ factor in the absence of the correlation contribution. Thereby, as has been originally demonstrated in [24,26], the emissivity of the process $p \rightarrow p\nu\bar{\nu}$ can be compatible with that for $n \rightarrow n\nu\bar{\nu}$ in dependence on the relation between Δ_p and Δ_n .

Inclusion of superfluid effects for rather low temperatures does not change our general conclusion. But very efficient processes become to be NPBF processes which compete with MMU processes. The former win the content for not too massive stars in agreement with the prediction of [24].

Pion (kaon) condensate processes. The pion condensate can be of three types: π_s^+ , π_s^\pm , and π^0 with different values of the critical densities $\rho_{c\pi} = (\rho_{c\pi^\pm}, \rho_{c\pi_s^+}, \rho_{c\pi^0})$, see [67]. Thus above the threshold density for the pion condensation of the given type, the neutrino emissivity of the MMU process (28) is to be supplemented by the corresponding PU processes

$$\begin{array}{c} \bar{\nu} \\ \swarrow \\ n \xrightarrow{e} p \xrightarrow{\pi_c^- (K_c^-)} n \end{array}, \quad \begin{array}{c} \bar{\nu} \\ \swarrow \\ n \xrightarrow{e} p \xrightarrow{\pi_c^+} n \end{array}, \quad \begin{array}{c} \bar{\nu} \\ \swarrow \\ n \xrightarrow{\nu} n \xrightarrow{\pi_c^0} n \end{array} \dots \quad (35)$$

To be specific, considering charged pion condensation we use a simplified expression including the nucleon–nucleon correlation effect in the πNN vertices [22,16],

$$\epsilon[\text{PU}] \simeq 1.5 \times 10^{27} \frac{p_{Fn}}{m_\pi} \frac{m_n^* m_p^*}{m_N^2} \gamma_\beta^2(p_{Fe}, p_{Fe}) \tilde{\gamma}^2(g', 0, p_{Fn}) T_9^6 \sin^2 \theta \frac{\text{erg}}{\text{cm}^3 \text{ sec}}. \quad (36)$$

Here $\rho > \rho_{c\pi}$ and $\sin \theta \simeq \sqrt{2|\tilde{\omega}^2|/m_\pi^2}$ for $\theta \ll 1$. Of the same order of magnitude are emissivities of other possible π condensate reactions. Since $\pi^{+,-}$ condensation probably reduces the energy gaps of the superfluid states by an order of magnitude, see [68], we may assume that superfluidity vanishes above $\rho_{c\pi}$. Finally we note that though the PU processes have genuinely one-nucleon phase-space volumes, their contribution to the resulting emissivity is suppressed relative to the DU by an additional $\tilde{\gamma}^2(g', 0, p_{Fn})$ suppression factor due to existence of the extra (πNN) vertex in the former case.

Fig. 4 compares the mass dependence of the neutrino cooling rates L_ν/C_V , L_ν is neutrino luminosity, C_V is the heat capacity, associated with MMU (MOPE) and MU (FOPE) for non-superfluid matter. For the solid curves, the neutrino emissivity in pion-condensed matter (to be conservative we took threshold density to be $3\rho_0$) is taken into account according to eq. (36) and (28) with the parameter $\alpha = \sqrt{2}$. Dashed curves correspond to the case where no pion condensation is allowed. As one sees, the medium polarization effects included in MMU may result in three order

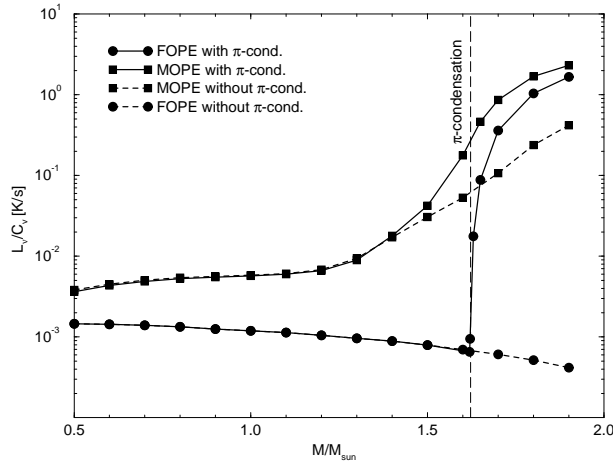


Fig. 4. Cooling rate due to neutrino emission as a function of star mass for a representative temperature of $T = 3 \times 10^8$ K. The solid curves refer to cooling via MU(FOPE) and MMU(MOPE). For $\rho > 3\rho_0$ PU is included. The dashed curves refer to cooling without PU. Superfluidity is neglected.

of magnitude increase of the cooling rate for the most massive stars. Even for stars of a rather low mass the cooling rate of MMU is still few times larger than for MU because even in this case the more efficient rate is given by the reactions shown by the right diagram in Fig.1 (first two diagrams of eq. (27)). The cooling rates of the $1.8M_\odot$ mass models with and without pion condensate differ only by a factor of 5 in this model. If we would take $\rho_{c\pi}$ to be smaller the ratio of emissivity PU to MMU would decrease and could even become $\lesssim 1$ in the vicinity of $\rho_{c\pi}$. One sees that the reaction rates for the FOPE model are rather independent of the star's mass for the stars with masses below the critical value $1.63M_\odot$, at which transition into the pion condensed phase occurs, and show a flattening behaviour above the critical mass. It is to be stressed that incorporation of pion condensation processes seems quite inconsistent, whether one applies FOPE model since pion condensation arises at $\rho > \rho_{c\pi}$ only as the consequence of the pion softening existed for $\rho < \rho_{c\pi}$. Opposite, the MOPE model [23] consistently takes into account the pion softening effects for $\rho < \rho_{c\pi}$ and both the pion condensation and pion softening effects on the ground of the condensate for $\rho > \rho_{c\pi}$. For $\rho > \rho_{cK}$ the kaon condensate processes come into play. Although kaon condensation can be of both S and P wave types [69], most popular is the idea of the S wave K^- condensation (e.g. see [13]) which is allowed at the condition $\mu_e > m_{K^-}^*$ due to the possibility of the reaction $e \rightarrow K^- \nu$. The corresponding condition for the pions $\mu_e > m_{\pi^-}^*$ is not fulfilled due to a strong S wave repulsion in the latter case. The neutrino emissivity of the K^- condensate processes (see first diagram of (35)) is given by equation analogous to (36) with a different NN correlation factor and an additional suppression factor due to a small contribution of the Kabibbo angle. However qualitatively scenarium that permits pion condensate processes is analogous for that with the kaon condensate processes.

Other resonance processes. There are many other reaction channels allowed in the medium. E.g any Fermi liquid allows for propagation of zero sound excitations of different symmetry related to the pion and the quanta of a more local interaction determined via $f_{\alpha,\beta}$ and $g_{\alpha,\beta}$. These excitations being present at $T \neq 0$ may par-

ticipate in the neutrino reactions. The most essential contribution comes from the neutral current processes [23] given by first two diagrams of the series

$$\dots + \dots \quad (37)$$

Here the dotted line is zero sound quantum of appropriate symmetry. These are the resonance processes of DU-type analogous to those processes going on the condensates with the only difference that the rates of reactions with zero sounds are proportional to the thermal occupations of the corresponding spectrum branches whereas the rates of the condensate processes are proportional to the modulus squared condensate mean field. Contribution of the resonance reactions is however rather small due to a small phase space volume ($q \sim T$) associated with zero sounds. Please also bear in mind an analogy with the processes (37) with the phonon processes in the crust.

DU processes. The proper DU processes in matter, as $n \rightarrow pe^- \bar{\nu}_e$ and $pe^- \rightarrow n\nu_e$

$$\dots + \dots \quad (38)$$

should also be treated with the full vertices. They are forbidden up to the density ρ_{cU} when triangle inequality $p_{Fn} < p_{Fp} + p_{Fe}$ begins to fulfill. For traditional equations of state like that given by the variational theory [18] DU processes are permitted for $\rho > 5\rho_0$. The emissivity of the DU processes renders

$$\epsilon^{DU} \simeq 1.2 \cdot 10^{27} \frac{m_n^* m_p^*}{m_N^2} \left(\frac{\mu_l}{100 \text{ MeV}} \right) \gamma_\beta^2 \min[\zeta(\Delta_n), \zeta(\Delta_p)] T_9^6 \frac{\text{erg}}{\text{cm}^3 \text{ sec}}, \quad (39)$$

where $\mu_l = \mu_e = \mu_\mu$ is the chemical potential of the leptons in MeV. In difference with the usually exploited result [15], eq. (39) contains a pre-factor γ_β^2 [26] due to taking into account of the NN correlations in the β decay vertices.

It was realized in ref. [70] that the softening of the pion mode in dense neutron matter could give rise to a rearrangement of single-particle degrees of freedom with an abnormal increase of the effective non-relativistic masses in a density interval $\rho_{cF} < \rho < \rho_{c\pi}$ that in its turn, opens a DU channel of neutrino cooling of neutron stars from the corresponding layer.

A rearrangement of single-particle degrees of freedom occurs if the necessary condition for stability of the normal state of a Fermi liquid is violated. At $T = 0$ this condition states that the change of the ground-state energy must remain positive for any admissible variation $\delta n(p)$ of the Landau quasiparticle distribution $n(p)$ away

from its normal-state form $\theta(p - p_F)$, i.e., $\delta E_0 = \int \xi(p, n(p)) \delta n(p) \frac{d^3 p}{(2\pi)^3} > 0$, where $\xi(p, n(p)) \equiv \varepsilon(p, n(p)) - \mu$ is the energy of a quasiparticle, measured from the chemical potential μ . This stability condition fails if a depression with $\xi < 0$ forms in the spectrum $\xi(p)$ at $p > p_F$; it likewise fails if there arises an elevation with $\xi > 0$ at $p < p_F$. The rearrangement is precipitated when the density ρ reaches a critical value ρ_{cF} where there emerges a new root $p = p_0$ of the equation $\xi(p, n(p); \rho_{cF}) = 0$, a relation that ordinarily serves merely specify the Fermi momentum p_F .

The nucleon quasiparticle spectrum is determined from the corresponding Dyson equation which in our MOPE model renders

$$\xi(p) = \xi^0(p) + \lambda^2 \int \frac{k_0^2}{\tilde{\omega}^2 + \gamma_m[(\vec{p} - \vec{k})^2 - k_0^2]^2 / 4k_0^2} n(k) \frac{d^3 k}{(2\pi)^3}, \quad (40)$$

where $\lambda^2 = f_{\pi N}^2 \gamma^2(g_{nn}, 0, k_0) m_N^* / m_N$, and we expanded the value $\tilde{\omega}^2(k)$ near k_0 , γ_m is the corresponding coefficient. Numerical study of [70] found the bifurcation point and documented three features of the rearrangement of the single-particle degrees of freedom. (i) The critical density ρ_{cF} for the rearrangement is less than the critical density $\rho_{c\pi}$ for pion condensation. Since both phenomena stem from the strong momentum dependence of the Landau amplitude, rearrangement of the quasiparticle distribution may be regarded as a *precursor* of pion condensation. (ii) The bifurcation point is positioned at $p_0 < 0.2p_F$ for the density interval under consideration. (iii) The ratios $\rho_c / \rho_{c\pi}$ and p_0 / p_F are insensitive to the actual value taken by $\rho_{c\pi}$ within the current range of theoretical predictions. (iiii) For the momenta above the bifurcation point $p > p_0$ there arises a dip in the profile $\xi(p)$ with a minimum at $p \sim 0.5p_{Fn}$.

An equation analogous to (40) can be applied to the proton subsystem of neutron-star matter. One is then dealing with the charged pion mode, and the neutrons form a strongly momentum-dependent external field in which the protons seek to occupy states with the lowest single-particle energies. The critical densities for neutral and charged pion condensation do not differ greatly, so we can appropriate the results obtained for neutron matter to argue that protons will leave the old Fermi sphere and occupy states of relatively large momentum in the region $p \sim 0.5p_{Fn}$. We defer here the impact of this further rearrangement.

Beyond the bifurcation point, the creation of a bubble at low neutron momenta in the Fermi sea means that the triangle inequalities are satisfied without the conventional requirement that the proton fraction exceeds some 11-14%, cf. [15]. Accordingly, the triangle condition for momentum conservation is readily met and the DU processes become active in the density regime just short of the threshold for pion condensation. The neutrino emissivity goes, as usual, like T^6 . Therefore the rearrangement of the neutron Fermi sphere that we have envisioned serves to turn on the DU process at a lower density.

There also exists a more radical scenario for rearrangement of the quasiparticle distribution [71–73]. In this case the condition $\xi = 0$, that has determined the bifurcation

point continues to fulfill in a density interval $\rho_{cF} < \rho < \rho_{c\pi}$ and in the corresponding finite momentum interval $p_i < p < p_f$. In this interval the occupancy $n(p)$ becomes partial, between 0 and 1 that determines the effective nonrelativistic mass relation to the temperature as $m_n^* \propto m_N \epsilon_F / T$. The family of quasiparticles having momenta $p \in [p_i, p_f]$ characterizing by dispersionless spectrum (at $T = 0$) has been called the fermion condensate because of a conspicuous analogy with the low-temperature Bose gas, where the energy of condensate particles is also equal to the chemical potential μ . It is worth noting that a key signature of fermion condensation has been observed in strongly correlated electron systems. Flat portions of the single-particle spectrum have been seen experimentally in a number of high-temperature superconductors ([74]), and this phenomenon has been linked to fermion condensation ([72]). Numerical studies [75] demonstrate that fermion condensate wins over the bubble formation at $T \neq 0$. Although the rearranged Fermi condensate momentum distribution differs from that of the bubble rearrangement, its structure will also permit thermal excitations to occur at low neutron momenta. Hence we may again expect most neutron stars to contain a region of relatively moderate density, bounded below by ρ_{cF} and above by $\rho_{c\pi}$, in which the DU process operates vigorously. However, due to the new feature of a temperature-dependent neutron effective mass, $M_n \propto 1/T$, we may anticipate an extra enhancement of the neutrino emissivity relative to the standard result of [15], corresponding to a reduction in the power of the temperature dependence from T^6 to T^5 . At early hot stage this layer becomes to be opaque to the neutrinos slowing the transport from the massive neutron star core to the exterior.

3.3 Comparison with soft X ray data

At first seconds-hours neutrino opacity effects become to be not efficient and the neutron star is transparent for neutrinos/antineutrinos. The heat transport within the crust establishes homogeneous density profile at times $\lesssim 10$ yr. After that time the subsequent cooling is determined by simple relation $C_V \dot{T} = -L$ where $C_V = \sum_i C_{V,i}$ and $L = \sum_i L_i$ are the sums of the corresponding partial contributions to the heat capacity (specific heat integrated over the volume) and the luminosity (emissivity integrated over the volume).

The nucleon pairing gaps are rather purely known. Therefore one may vary them. The "standard" and "nonstandard" scenarios of the cooling of neutron stars of several selected masses for suppressed gaps are demonstrated in the left panel of Fig. 5, [26]. Depending on the star's mass, the resulting photon luminosities are basically either too high or too low to account for the bulk of observed pulsar luminosities. Situation changes, if the MMU-process with the medium modifications of the pion exchange interaction, appropriate vertex corrections, and the radiation from intermediate reaction states [23,16] is included. Now, the cooling rates vary smoothly with the star mass (see right panel of Fig. 5) such that the gap between standard and enhanced cooling is washed out. More quantitatively, by means of varying the

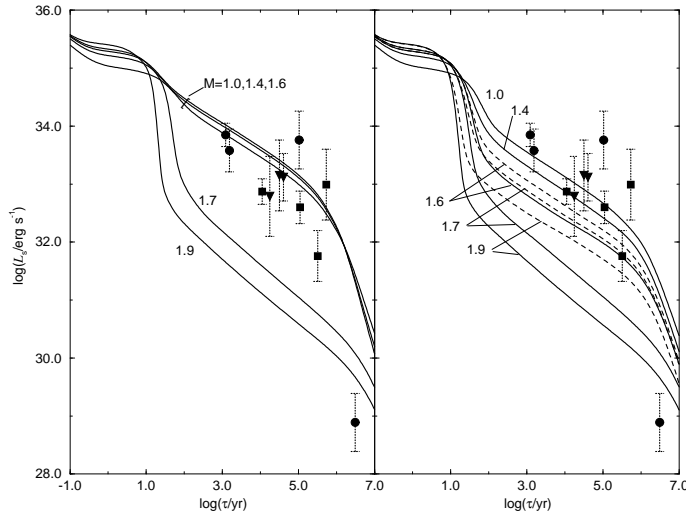


Fig. 5. Cooling of non-superfluid neutron star models of different masses constructed for the HV EOS. The two graphs refer to cooling via MU(FOPE) + PU (left) and MMU(MOPE)+PU (right). In both cases, pion condensation is taken into account for the solid curves where $\rho > \rho_{c\pi}$ chosen to be $3\rho_0$. The dashed curves in the right graph refer to the $\tilde{\omega}^2(p_{Fn})$ parametrization without pion condensation. The observed luminosities are labeled by dots. Possibility of Fermi sea rearrangement is suppressed.

star's mass between $1 - 1.6 M_{\odot}$, one achieves an agreement with a large number of observed data points. This is true for both choices of the $\tilde{\omega}^2$ parameterization, independently whether pion (kaon) condensation can occur or not. Two parameterizations differ only in the range which is covered by the cooling curves. The only point which does not agree with the cooling curves belongs to the hottest pulsar PSR 1951+32. Other three points which according to Fig. 5, right panel, are also not fitted by the curves can be, nevertheless, fitted introducing slight changes of the parameters of the model. The high luminosity of PSR 1951+32 may be due to internal heating processes, which lead to a delayed cooling for star ages $t > 10^5$ yr, cf. [10].

We turn now to cooling simulations where the MU, NPB, DU and PU take place simultaneously. Parameters of the pairing gaps are from Fig. 6 of ref. [26]. Fig. 6 shows the cooling tracks of stars of different masses, computed for the HV equation of state. Possibility of Fermi sea rearrangement is suppressed. Very efficient at $T < T_c$ become to be NPB processes which compete with MMU processes. The former win the content for not too massive stars in agreement with prediction of [24]. The DU process is taken into account in the right graph, whereas it is neglected in the left graph. The solid curves refer again to the $\tilde{\omega}^2$ -parameterization with phase transition to a pion condensate, the dashed curves to the one without phase transition. For masses in the range between 1.0 and $1.6 M_{\odot}$, the cooling curves pass through most of the data points. We again recognize a photon luminosity drop by more than two orders of magnitude of the $1.7 M_{\odot}$ mass star with pion condensate, due to vanishing of the superfluidity as a consequence of pion condensation. This drop is even larger if the DU is taken into account (right graph, this allows to account for the photon luminosity of PSR 1929+10).

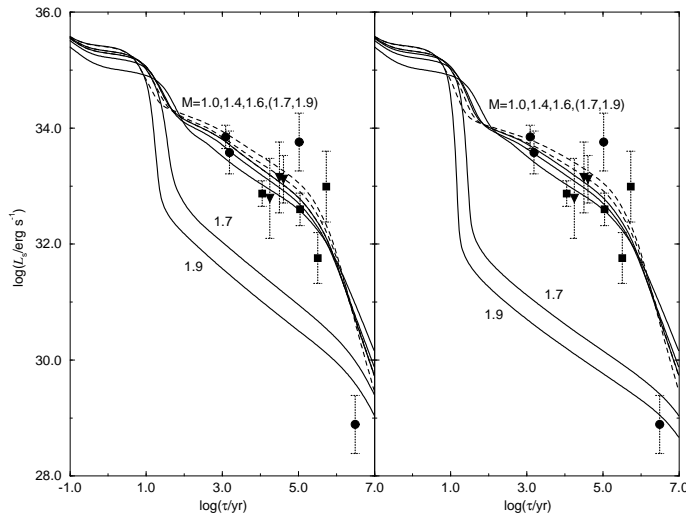


Fig. 6. Cooling of neutron stars with different masses constructed for the HV EOS. The cooling processes are MU-VS86, PU (only solid curves), NPBF, PPBF, and DU (only in the right graph). The dashed curves refer to the $M = 1.7$ and $1.9M_{\odot}$ models without pion condensate.

A comparison with the observed luminosities shows that one gets quite good agreement between theory and observation if one includes into consideration all available in-medium effects assuming that the masses of some of the underlying pulsars are different from the canonical value, $M = 1.4 M_{\odot}$. Since the masses of these pulsars are not known, no further conclusions about the actually operating cooling mechanism of these pulsars can be drawn yet. Future mass determinations of these objects will change the situation.

Thus, ref. [26] demonstrated that the data can be treated with the help of the model based on the results which incorporate most important in-medium effects. We also point out that the description of these effects is constructed in essentially the same manner for all the hadron systems as neutron stars, atomic nuclei and heavy ion collisions, cf. [16].

3.4 Neutrino opacity

Important part of in-medium effects for description of neutrino transport at initial stage of neutron star cooling was discussed in [23,24,16], where correlation effects, pion softening and pion condensation, the latter for $\rho > \rho_c$, were taken into account. The neutrino and antineutrino mean free paths can be evaluated from the corresponding kinetic equations via the neutrino/antineutrino widths $\Gamma_{\nu(\bar{\nu})} = -2\text{Im}\Pi_{\nu(\bar{\nu})}^R$, where Π^R is the retarded selfenergy, or within the quasiparticle approximation for the nucleons they can be calculated via the squared matrix elements of the corresponding reactions. Thereby the processes which the most efficiently contribute to the emissivity (at $T \sim 1\text{MeV}$ typical for the value of T_{opac}) are at early times responsible for the opacity.

In above scenarium at $T > T_c$ the most essential contribution was given by MMU. Taking into account of nucleon–nucleon correlations in the vertices of two-nucleon processes like MMU and MNB suppresses the rates, whereas account of the pion softening in the pion propagator leads to their essential enhancement. For rather massive neutron stars MOPE wins the competition. The mean free path of neutrino/antineutrino in MMU processes is determined by the same diagrams (27) as the emissivity. Its calculation with the two first diagrams gives the following evaluation (see (28))

$$\frac{\lambda_\nu^{MMU}}{R} \simeq \frac{1.5 \cdot 10^5}{F_1(2\Gamma)^8 T_9^4} \left(\frac{\rho_0}{\rho} \right)^{10/3} \frac{m_N^4}{(m_n^*)^3 m_p^*} \left[\frac{\alpha \tilde{\omega}_{\pi^0}(p_{Fn})}{m_\pi} \right]^4 \left[\frac{\alpha \tilde{\omega}_{\pi^\pm}(p_{Fn})}{m_\pi} \right]^4. \quad (41)$$

From the relation $\lambda_\nu \simeq R$ follows evaluation of T_{opac} . With the only first diagram we get a simple relation

$$T_9^{opac} \simeq 15 \frac{\rho_0}{\rho} \frac{\tilde{\omega}^2(p_{Fn})}{(2\Gamma)^{3/2}} \frac{m_N}{m_N^*} \quad (42)$$

For averaged value of the density $\rho \simeq \rho_0$ corresponding to medium heavy neutron stars ($< 1.4 M_\odot$) with $\tilde{\omega}^2(p_{Fn}) \simeq 0.8 m_\pi^2$, $\Gamma \simeq 0.4$ we get $T_{opac} \simeq 1.5 \text{ MeV}$ that is still smaller then the corresponding value 22 MeV estimated with FOPE. For $\rho \simeq 2\rho_0$ that corresponds to a more massive neutron star we evaluate $T_{opac} \simeq 0.5 \text{ MeV}$. Thus pion softening results in a substantial decrease of neutrino path lengths for typical energy $\sim T$ and the value of T_{opac} .

The diffusion equation determins the characteristic time scale for the heat transport of neutrinos from the hot zone to the star surface $t_0 \sim R^2 C_V \sigma^{-1} T^{-3} / \lambda_\nu$, whereas it follows that $t_0 \sim 10 \text{ min.}$ for $T \simeq 10 \text{ MeV}$ and $\rho \simeq \rho_0$, $\tilde{\omega}^2 \simeq 0.8 m_\pi^2$, $\Gamma \simeq 0.4$, $m_N^*/m_N \simeq 0.9$ and $t_0 \sim$ becomes as large as several hours for $\rho \simeq 2 \div 3 \rho_0$. These estimates demonstrate that more massive neutron stars cool down more slowly at $T > T_{opac}$ and faster at subsequent times then the less massive stars.

Due to in-medium effects neutrino scattering cross sections on the neutrons shown by the first diagram (19) require the factor

$$\gamma_{n\nu}^2(\omega, q) = \frac{\gamma^2(f_{nn}, \omega, q) + 3g_A^2 \gamma^2(g_{nn}, \omega, q)}{1 + 3g_A^2}, \quad (43)$$

due to nucleon-nucleon correlations, as follows from eq. (17). This results in the corresponding suppression factor $0.5 \div 0.7$ of the cross sections. Neutrino scattering cross sections on the protons are modified differently, by

$$\gamma_{p\nu}^2(\omega, q) = \frac{\kappa^2(f_{np}, f_{nn}, \omega, q) + 3g_A^2 \gamma_{pp}^2(g_{nn}, \omega, q)}{1 + 3g_A^2}, \quad (44)$$

that leads to analogous estimate of their contribution to the cross sections of the $\nu p \rightarrow \nu p$ processes.

Also there is an additional suppression of the νN scattering and MNB reaction rates for soft neutrinos ($\omega \lesssim 3T$) due to multiple NN collisions as

(45)

(Landau–Pomeranchuk–Migdal effect). One may qualitatively estimate these effects multiplying the corresponding squared matrix elements by suppression factor $C_0(\omega) = \omega^2/[\omega^2 + \Gamma_N^2]$ where Γ_N is the nucleon width and the ω is the energy of $\nu\bar{\nu}$ or $\nu\nu$ pair. However in general the prefactors are different for different diagrams under consideration. They follow from derivation from the general result [28]. Factor like C_0 was used in refs [78,79] being introduced there at ansatz level. One does not need any ansatz reductions. *Optical theorem formalism suggested in*, see [28], *allows to calculate the rates using the exact sum rule!* The modification of the charged current processes is unimportant since the corresponding ω is $\simeq p_{Fe} \gg \Gamma_N$.

The main physical result is that *besides a suppression due to nucleon correlations and infra-red pre-factors, there exists an enhancement due to pion softening*. The latter demonstrates that for densities $\rho > \rho_{c1} \sim (0.5 - 0.7)\rho_0$ nucleon system begins to feel that it may have π condensate phase transition for $\rho > \rho_c$, although this ρ_c value might be essentially larger than the value ρ_{c1} .

4 How to calculate the rate of radiation from dense medium

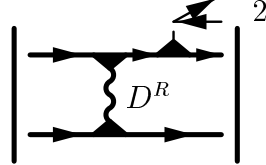
Quasiparticle approximation for fermions is applicable if the fermion width is much less than all the typical energy scales essential in problem under consideration $\Gamma_F \ll \omega_{ch}$. In calculation of the emissivities of $\nu\bar{\nu}$ reactions the minimal scale is $\omega_{ch} \simeq 3T$, averaged energy typical for MNB reactions. For MMU it is $\simeq p_{Fe}$. For radiation of soft quanta of fixed energy $\omega < T$ it is ω . Within quasiparticle approximation for fermions the reaction rate with participation of in-medium fermion and in-medium boson is given by [22,23]

(46)

For equilibrium ($T \neq 0$) system there is the strict relation

$$(\langle \hat{\varphi}_2^\dagger \hat{\varphi}_1 \rangle)(p) = iD^{-+} = \frac{\Gamma_B}{\exp(\frac{\omega}{T}) - 1}, \quad \Gamma_B = -2\text{Im}D^R, \quad (47)$$

where $(\langle \hat{\varphi}_2^\dagger \hat{\varphi}_1 \rangle)(p)$ means the Fourier component of the corresponding non-equilibrium Green function. Thus the rate of the reaction is related to the boson width being determined by the corresponding Dyson equation for D^{-+} having the form (9). The boson width Γ_B is non-zero at the spectrum branches related to resonance processes, like zero sound. The poles related to upper branches do not contribute at small temperatures due to a tiny thermal population of those branches. There is also a contribution to $\text{Im}D^R$ proportional to $\text{Im}\Pi^R$ given by the particle-hole diagram. Taking Im part means the cut of the diagram. Thus we show [23] that this contribution is the same as that could be calculated with the help of the squared matrix element of the two-nucleon process


(48)

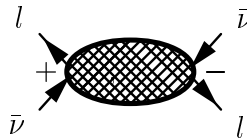
This is precisely what one could expect using the optical theorem. Thus unlimited series of all possible diagrams with in-medium Green functions (see (19), (35), (37), (38)) together with two-fermion diagrams (as given by (27)) and multiple-fermion diagrams (like (45)) would lead us to a double counting. The reason is that permitting the boson width effects (and beyond the quasiparticle approximation for fermions also permitting finite fermion width) the difference between one-fermion, two-fermion and multiple-fermion processes in medium is smeared out. All the states can still participate in subsequent production and absorption processes. Within quasiparticle approximation for fermions these further processes are suppressed for fermions (due to assumption $\Gamma_F \ll \epsilon_{ch}$) but allowed for the bosons. Staying with the quasiparticle picture for fermions, the easiest way to avoid mentioned double counting is just to calculate the reaction rates according to (46) thus with the help of the diagrams of the DU-like type, which already include all the contributions of the two-nucleon origin. On other hand, it is rather inconvenient to explicitly treat all one-nucleon processes dealing with different specific quanta instead of a more convenient treatment of the full NN interaction like in (48) which has a complicated structure. Besides, as we have mentioned, consideration of open fermion legs is only possible within the quasiparticle approximation for fermions since Feynman technique is not applicable anymore if Green functions corresponding to ingoing and outgoing fermions have widths that in other language means possibility of additional processes. Thus the idea came [24,28] to integrate over all in-medium states allowing all possible processes instead of specifying different special reaction channels.

In refs [24,28,27] it was shown that OTF in terms of non-equilibrium Green's functions is efficient tool to calculate the reaction rates including finite particle widths and other in-medium effects. Applying this approach to the anti-neutrino-lepton (electron, μ^- meson, or neutrino) production [24] we can express the transition probability in a direct reaction in terms of the evolution operator S

$$\frac{d\mathcal{W}_{X \rightarrow \bar{\nu}l}^{\text{tot}}}{dt} = \frac{(1 - n_l) dp_l^3 dp_{\bar{\nu}}^3}{(2\pi)^6 4 E_l E_{\bar{\nu}}} \sum_{\{X\}} \overline{\langle 0 | S^\dagger | \bar{\nu}l + X \rangle \langle \bar{\nu}l + X | S | 0 \rangle}, \quad (49)$$

where we write explicitly the phase-space volume of $\bar{\nu}l$ states; lepton occupations of given spin, n_l , should be put zero for ν which are supposed to be radiated directly from the system. The bar denotes statistical averaging. The summation goes over complete set of all possible intermediate states $\{X\}$ constrained by the energy-momentum conservation law. It was also supposed that electrons (and muons) can be treated in the quasiparticle approximation, i.e. with zero widths. Thus, although possible, there is no need to consider them in intermediate reaction states. Making use of the smallness of the Fermi weak-interaction constant G , we expand the evolution operator as $S \approx 1 - i \int_{-\infty}^{+\infty} T \{V_W(x) S_{\text{nucl}}(x)\} dx_0$, where V_W is the Hamiltonian of the weak interaction, in the interaction representation, S_{nucl} is the part of the S matrix corresponding to the nuclear interaction, and $T\{\dots\}$ stands for the chronological ordering operator. After substitution of this S matrix into Eq. (49) and averaging over the arbitrary non-equilibrium state of a nuclear system, there appear chronologically ordered (G^{--}), anti-chronologically ordered (G^{++}) and disordered (G^{+-} and G^{-+}) exact Green functions.

In graphical form the general expression for the probability of the lepton (electron, muon, neutrino) and anti-neutrino production is determined by the diagram

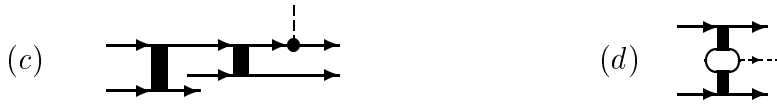


which represents the sum of all closed diagrams ($-i\Pi^{--}$) containing at least one $(-+)$ line. We will deal with full Green's functions and we will explicitly present all the contributions containing full G^{+-} and G^{-+} Green's functions, cf. [28]. Then the contributions of specific processes contained in a closed diagram can be made visible by cutting the diagrams over the $(+-)$, $(-+)$ lines. In the framework of the quasiparticle approximation for the fermions (nucleons in our case) $G^{-+} = -\pi\delta(\epsilon + \mu - \epsilon_p^0 - \text{Re}\Sigma^R(\epsilon + \mu, \vec{p}))$ and the cut eliminating the energy integral thus has clear meaning. This way one establishes the correspondence between closed diagrams and usual Feynman amplitudes. In general case of finite fermion width the cut has only a symbolic meaning.

Various contributions from $\{X\}$ can be classified according to the number N of G^{-+} lines in the diagram. We can write, e.g.,

$$\frac{d\mathcal{W}_{\bar{\nu}l}^{\text{tot}}}{dt} = \frac{d^3q_{\bar{\nu}}dq_l^3}{(2\pi)^6 4\omega_{\bar{\nu}}\omega_l} \left(\begin{array}{c} l \\ \nearrow \\ + \\ \nwarrow \\ \bar{\nu} \end{array} \begin{array}{c} \text{---} \\ \text{---} \\ \text{---} \\ \text{---} \end{array} \begin{array}{c} \nwarrow \\ - \\ \nearrow \\ l \end{array} \begin{array}{c} \bar{\nu} \end{array} + \begin{array}{c} l \\ \nearrow \\ + \\ \nwarrow \\ \bar{\nu} \end{array} \begin{array}{c} \text{---} \\ \text{---} \\ \text{---} \\ \text{---} \end{array} \begin{array}{c} \nwarrow \\ - \\ \nearrow \\ l \end{array} \begin{array}{c} \bar{\nu} \end{array} \dots \right). \quad (50)$$

This procedure suggested in [24] is actually very helpful especially if the quasiparticle or quasiclassical approximations hold for the fermions (for $\omega_l + \omega_{\bar{\nu}} \sim T \gg \Gamma_F$, where $\Gamma_F \sim T^2/\epsilon_F$ is the fermion (nucleon) width). E.g. in the quasiparticle approximation any extra G^{-+} brings a small $(T/\epsilon_F)^2$ factor to the emissivity of the process. Dealing with small temperatures one can restrict by the diagrams of the lowest order in $(G^{-+}G^{+-})$ not forbidden by energy-momentum conservations putting $T = 0$ in all G^{++} and G^{--} Green functions.



The full circle denotes the effective weak coupling vertex. The one-loop diagram in (52) is particular, since its quasiparticle approximant in many cases vanishes as we have mentioned. However the full one-loop includes quasiparticle graphs of the type (53b), which survive to the same order in $\Gamma/\bar{\epsilon}$ as the other diagrams (therefore in [24] where quasiparticle picture was used this diagram was considered as allowed diagram). In quasiparticle series such a term should be included in second diagram of (refqp) although beyond the quasiparticle approximation it should be included as self-energy insertion to the one-loop result [28]. In fact it is positive definite and corresponds to the absolute square of the amplitude (53a)). The other diagrams 2, 4 and 5 of (52) describe the interference of amplitude (53a) either with those where the weak coupling quantum couples to another leg or with one of the exchange diagrams. Thereby for neutral interactions diagram (52:2) is more important than diagram 4, while this behavior reverses for charge exchange interactions (the latter is also important for gluon radiation from quarks in QCD transport due to color exchange interactions). Diagrams like 3 describe the interference terms due to further rescatterings of the source fermion with others as shown by (53c). Diagram (52:6) describes the production from intermediate states and is given by Feynman graph (53d). For photons in the soft limit ($\omega_q \ll \epsilon_F$) this diagram (53d) gives a smaller contribution to the photon production rate than the diagram (53a) in quasiparticle approximation, where the normal bremsstrahlung contribution diverges like $1/\omega_q$ compared to the $1/\epsilon_F$ -value typical for the coupling to intermediate fermion lines [23]. For $\nu\bar{\nu}$ bremsstrahlung it gives zero. However in some specific cases the process (53d) might be very important even in the soft limit. This is indeed the case for MMU process which is of prime importance in the problem of neutrino radiation from the dense neutron star interior. Some of the diagrams which are not presented explicitly in eq.(52) give more than two pieces, if being cut, so they do not reduce to the Feynman amplitudes.

With $\Gamma_F \sim \pi^2 T^2 / \epsilon_F$ for Fermi liquids, the quasiparticle approximation for fermions constitutes a consistent scheme for all thermal excitations $\Delta\epsilon \sim T \ll \epsilon_F$. However with the application to radiation at somewhat higher temperatures this concept is no longer justified. In particular, the remaining series of quasiparticle-diagrams is *no longer convergent* unless $\omega > \Gamma_F$, since arbitrary powers in Γ_F/ω appear, and there is no hope to ever recover a reliable result by a finite number of quasiparticle diagrams for the production of soft quanta! With *full Green's functions*, however, one obtains a description that uniformly covers both the soft ($\omega \ll \Gamma_F$) and the hard ($\omega \gg \Gamma_F$) regime.

In order to correct quasiparticle evaluations of different diagrams by the fermion width effects for soft radiating quanta one can simply multiply the quasiparticle results by different pre-factors [28]. E.g., comparing the one-loop result at non-zero Γ_F with the first non-zero diagram in the quasiparticle approximation ($\Gamma_F = 0$ in

the fermion Green's functions) we get

$$\text{---}\overset{+}{\bullet}\text{---}\text{---}\overset{-}{\bullet}\text{---} = C_0(\omega) \left\{ \text{---}\overset{+}{\bullet}\text{---}\text{---}\overset{-}{\bullet}\text{---} \right\}_{\text{QPA}}, \quad (54)$$

at small momentum \vec{k} where C_0 is given by (??) which cures the defect of the QPA for soft ω . This factor complies with the replacement $\omega \rightarrow \omega + i\Gamma$. A similar factor has been observed in the diffusion result, where however the macroscopic relaxation rate Γ_x enters, due to the resummation of all rescattering processes.

Along similar routes the correction factors for the higher order diagrams can be derived. For the next order diagrams we have

$$\text{---}\overset{+}{\bullet}\text{---}\text{---}\overset{-}{\bullet}\text{---} = C_1(\omega) \left\{ \text{---}\overset{+}{\bullet}\text{---}\text{---}\overset{-}{\bullet}\text{---} \right\}_{\text{QPA}}, \quad C_1(\omega) = \omega^2 \frac{\omega^2 - \Gamma^2}{(\omega^2 + \Gamma^2)^2}, \quad (55)$$

$$\text{---}\overset{+}{\bullet}\text{---}\text{---}\overset{-}{\bullet}\text{---} = C_0(\omega) \left\{ \text{---}\overset{+}{\bullet}\text{---}\text{---}\overset{-}{\bullet}\text{---} \right\}_{\text{QPA}}, \quad C_0(\omega) = \frac{\omega^2}{\omega^2 + \Gamma_N^2}. \quad (56)$$

In the quasiclassical limit for fermions (with occupations $n_F \simeq \exp((\epsilon - \mu_F)/T)$) all the diagrams given by first line of series (52) with an arbitrary number of $-+NN-$ interaction insertions can be summed up leading to the diffusion result. For small momenta \vec{q} this leads to a suppression factor of the form $C = \omega^2/(\omega^2 + \Gamma_x^2)$. In general case the total radiation rate result is obtained by summation of all diagrams in (52).

Concluding, we demonstrated how to calculate the rates of different reactions in dense equilibrium (and non-equilibrium) matter and compared the results derived in closed diagram technique with those obtained in the standard technique of computing of the squared matrix elements. The *nuclear medium cooling scenario* allows easily to achieve agreement with existing data. However there remains essential uncertainty in quantitative predictions due to a pure knowledge of the residual interaction above treated within a phenomenological Fermi liquid model.

Acknowledgement: Author appreciates the hospitality and financial support of GSI Darmstadt and ETC* Trento. He also acknowledges J. Knoll and E. Kolomeitsev for the help.

References

- [1] S. Shapiro and S.A. Teukolsky, Black Holes, White Dwarfs and Neutron Stars: The Physics of Compact Objects, Wiley, N.Y. (1983), chapter 1.

- [2] D. Pines, R. Tamagaki and S. Tsuruta (eds.), Neutron Stars, Addison-Weseley, N.Y. (1992).
- [3] M. A. Alpar, Ü. Kiziloglu, and J. van Paradijs, eds. 1995, The Lives of the Neutron Stars (NATO ASI Ser. C, 450; Dordrecht: Kluwer).
- [4] J.N. Bahcall and R.A. Wolf, Phys. Rev. **B 140**, 1445 (1965).
- [5] S. Tsuruta and A.G.W. Cameron, Canad. J. Phys. **43**, 2056 (1965).
- [6] B. Friman and O.V. Maxwell, Ap. J. **232**, 541 (1979).
- [7] O.V. Maxwell, Ap. J. **231**, 201 (1979).
- [8] S. Tsuruta, Phys. Rep. **56**, 237 (1979).
- [9] K. Nomoto and S. Tsuruta, Ap. J. Lett. **250**, 19 (1981).
- [10] Ch. Schaab, F.Weber, M.K. Weigel, and N.K. Glendenning, Nucl. Phys. **A605**, 531 (1996).
- [11] G. Flowers, P.G. Sutherland, and J.R. Bond, Phys. Rev. **D 12**, 315 (1975).
- [12] O. Maxwell, G.E. Brown, D. Campbell, R. Dashen, and J. Manassah, Ap. J. **216**, 77 (1977).
- [13] G.E. Brown, K. Kubodera, D. Page, P. Pizzochero, Phys. Rev. **D 37**, 2042 (1988).
- [14] T. Tatsumi, Prog. Theor. Phys. **88**, 22 (1988).
- [15] J.M. Lattimer, C.J. Pethick, M. Prakash, and P. Haensel, Phys. Rev. Lett. **66**, 2701 (1991).
- [16] A.B. Migdal, E.E. Saperstein, M.A. Troitsky and D.N. Voskresensky, Phys. Rep. **192**, 179 (1990).
- [17] T. Takatsuka, and R. Tamagaki, Prog. Theor. Phys. **97**, 1, (1997).
- [18] A. Akmal, V.R. Pandharipande, and D.G. Ravenhall, Phys. Rev. **C 58**, 1804 (1998).
- [19] T. Suzuki, H. Sakai, and T. Tatsumi, nucl-th/9901097.
- [20] G.E. Brown, C.H. Lee, M. Rho, V. Thorsson, Nucl. Phys. **A567**, 937 (1994).
- [21] E.E. Kolomeitsev, D.N. Voskresensky, B. Kämpfer, Nucl. Phys. **A588**, 889 (1995).
- [22] D.N. Voskresensky and A.V. Senatorov, JETP Lett. **40**, 1212 (1984).
- [23] D.N. Voskresensky and A.V. Senatorov, JETP **63**, 885 (1986).
- [24] D.N. Voskresensky and A.V. Senatorov, Sov. J. Nucl. Phys. **45**, 411 (1987).
- [25] A.V. Senatorov and D.N. Voskresensky, Phys. Lett. **B 184**, 119 (1987).
- [26] Ch. Schaab, D. Voskresensky, A.D. Sedrakian, F.Weber and M.K. Weigel, Astron. Astrophys. **321**, 591 (1997).
- [27] E.E. Kolomeitsev and D.N. Voskresensky, Phys. Rev. **C 60**, 034610 (1999).

- [28] J. Knoll and D. N. Voskresensky, Phys. Lett. **B 351**, 43 (1995); Ann. Phys. (N. Y.) **249**, 532 (1996).
- [29] N.K. Glendenning, Phys. Rev. **D 46**, 1274 (1992).
- [30] M.B. Christiansen and N.K. Glendenning, astro-ph/0008207.
- [31] T. Tatsumi, Prog. Theor. Phys. **69**, 1137 (1983).
- [32] E. Flowers, M. Ruderman, P. Sutherland, Ap. J. **205**, 541 (1976).
- [33] D.G. Yakovlev, K.P. Levenfish, and Yu.A. Shibano, Phys. Usp. **169**, 825 (1999).
- [34] D. Page, Many Faces of Neutron Stars (Eds R. Buccheri, J. van Paradijs, M.A. Alpar) (Kluwer, Dordrecht, 1998) p. 538.
- [35] D.G. Yakovlev, A.D. Kaminker, and K.P. Levenfish, Astron. Astrophys. **343**, 650 (1999).
- [36] K.P. Levenfish and D.G. Yakovlev, Astron. Reports, **38**, 247 (1994).
- [37] R.F. Sawyer and A. Soni, Ap. J. **230**, 859 (1979).
- [38] R.F. Sawyer, Ap. J. **237**, 187 (1980).
- [39] R.F. Sawyer and A. Soni, Ap. J. **216**, 73 (1977).
- [40] S. Reddy and M. Prakash, Ap.J. **423**, 689 (1997).
- [41] J.A. Pons, S. Reddy, M. Prakash, J.M. Lattimer, and J.A. Miralles, Ap.J. **513**, 780 (1999).
- [42] D.N. Voskresensky, A.V. Senatorov, B. Kämpfer, and H. Haubold, Astrophys. Space Sci. **138**, 421 (1987).
- [43] H. Haubold, B. Kämpfer, A.V. Senatorov, and D.N. Voskresensky, Astron. Astrophys. **191**, L22 (1988).
- [44] A.B. Migdal. ZhETF. **61**, 2209 (1971) (in Engl.: JETP. **34**, 1184 (1972)).
- [45] A.B. Migdal, Rev. Mod. Phys. **50**, 107 (1978).
- [46] L.D. Landau, Sov. JETP. **3**, 920 (1956).
- [47] A.B. Migdal, Theory of Finite Systems and Properties of Atomic Nuclei, Willey and Sons, N.Y. (1967); second. ed. (in Russian), Nauka, Moscow, (1983).
- [48] E.E. Saperstein and S.V. Tolokonnikov, JETP Letters. **68**, 553 (1998).
- [49] S.A. Fayans and D. Zawischa, Phys. Lett. **B 363**, 12 (1995).
- [50] I.N. Borzov, S.V. Tolokonnikov and S.A. Fayans, Sov. J. Nucl. Phys. **40**, 732 (1984).
- [51] A.M. Dyugaev, Pisma v ZhETF. **22**, 181 (1975).
- [52] D.N. Voskresensky and I.N. Mishustin, JETP Lett. **34**, 303 (1981); Sov. J. Nucl. Phys. **35**, 667 (1982).

- [53] A.M. Dyugaev, Pisma v ZhETF. **35**, 341 (1982); ZhETF. **83**, 1005 (1982); Sov. J. Nucl. Phys. **38**, 680 (1983).
- [54] D.N. Voskresensky, E.E. Kolomeitsev, and B. Kämpfer, JETP. **87**, 211 (1998).
- [55] L.B. Leinson, Phys. Lett. **B473**, 318 (2000).
- [56] A.P. Platonov, E.E. Saperstein, S.V. Tolokonnikov, and S.A. Fayans, Phys. Atomic Nuclei, **58**, 556 (1995).
- [57] G.F. Bertsch, L. Frankfurt and M. Strikman, Science. **259**, 773 (1993).
- [58] G.E. Brown, M. Buballa, Zi Bang Li and J. Wambach, Nucl. Phys. **A593**, 295 (1995).
- [59] M. Ericson, Nucl. Phys. **A 577** (1994) 147c.
- [60] J. Delorm, M. Ericson, Phys. Rev. **C 49** (1994) 1763.
- [61] E. Marco. E. Oset and P. Fernandez de Cordoba, Nucl.Phys. **A 611**, 484 (1996).
- [62] E. Marco and E. Oset, Nucl.Phys. **A645**, 303 (1999).
- [63] S.V. Akulinichev, nucl-th/9502026, 1995.
- [64] C. Hanhart, D. R. Phillips, and S. Reddy, e-Print Archive: nucl-th/0003445.
- [65] D. Blaschke, G. Röpke, H. Schulz, A. Sedrakian, and D.N. Voskresensky, MNRAS, **273**, 596 (1995).
- [66] A.B. Migdal, Rev. Mod. Phys. **50**, 108 (1978).
- [67] T. Takatsuka, R. Tamagaki, Progr. Theor. Phys., **64**, 2270 (1980).
- [68] D.N. Voskresensky, V. A. Khodel, M. V. Zverev, and J.W. Clark, Ap. J. Lett. **533**, 127 (2000).
- [69] V. A. Khodel and V. R. Shaginyan, JETP Lett. **51**, 553 (1990).
- [70] P. Nozieres, J. Phys. I France **2**, 443 (1992).
- [71] V. A. Khodel, V. R. Shaginyan, and V. V. Khodel, Phys. Rep. **249**, 1 (1994).
- [72] Z. X. Shen and D. S. Dessau, Phys. Rep. **B 351**, 43 (1995).
- [73] M. V. Zverev and M. Baldo, JETP **87**, 1129 (1998).
- [74] A. Sedrakian and A. Dieperink, Phys. Lett. **B 463**, 145 (1999), nucl-th/0005029.
- [75] S.Yamada, Nucl. Phys. **A662**, 219 (2000).
- [76] G. Raffelt and D. Seckel, Phys. rev. **D 52** (1995) 1780.
- [77] S. Hannestad and G. Raffelt, astro-ph/971132.